Ecological Informatics 82 (2024) 102738

Contents lists available at ScienceDirect

Ecological Informatics

journal homepage: www.elsevier.com/locate/ecolinf

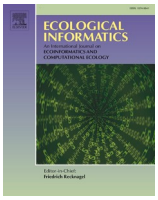

Landsat images and GIS techniques as key tools for historical analysis of landscape change and fragmentation

Darwin Gómez-Fernández [a,b,*], Rolando Salas López [a], Jhon A. Zabaleta-Santisteban [a], Angel J. Medina-Medina [a], Malluri Goñas [a,b], Jhonsy O. Silva-López [a,c], Manuel Oliva-Cruz [a], Nilton B. Rojas-Briceño [a,d]

[a] Instituto de Investigación para el Desarrollo Sustentable de Ceja de Selva (INDES-CES), National University Toribio Rodríguez de Mendoza (UNTRM), Chachapoyas 01001, Peru
[b] Centro Experimental Yanayacu, Dirección de Supervisión y Monitoreo en las Estaciones Experimentales Agrarias, Instituto Nacional de Innovación Agraria (INIA), Carretera Jaén San Ignacio KM 23.7, Jaén 06801, Cajamarca, Peru
[c] Laboratorio de Agrostología – AGROLAB, Facultad de Ingeniería Zootecnista, Agronegocios y Biotecnología, UNTRM, Chachapoyas 01001, Peru
[d] Escuela Profesional de Ingeniería Ambiental, Facultad de Ingeniería y Arquitectura, Universidad Nacional de Moquegua, Pacocha 18610, Peru

ARTICLE INFO

Keywords:
Fragmentation
LULC
Changes
Classification
Random Forest
Amazon
Forest

ABSTRACT

Monitoring and evaluation of landscape fragmentation is important in numerous research areas, such as natural resource protection and management, sustainable development, and climate change. One of the main challenges in image classification is the intricate selection of parameters, as the optimal combination significantly affects the accuracy and reliability of the final results. This research aimed to analyze landscape change and fragmentation in northwestern Peru. We utilized accurate land cover and land use (LULC) maps derived from Landsat imagery using Google Earth Engine (GEE) and ArcGIS software. For this, we identified the best dataset based on its highest overall accuracy, and kappa index; then we performed an analysis of variance (ANOVA) to assess the differences in accuracies among the datasets, finally, we obtained the LULC and fragmentation maps and analyzed them. We generated 31 datasets resulting from the combination of spectral bands, indices of vegetation, water, soil and clusters. Our analysis revealed that dataset 19, incorporating spectral bands along with water and soil indices, emerged as the optimal choice. Regarding the number of trees utilized in classification, we determined that using between 10 and 400 decision trees in Random Forest classification doesn't significantly affect overall accuracy or the Kappa index, but we observed a slight cumulative increase in accuracy metrics when using 100 decision trees. Additionally, between 1989 and 2023, the categories Artificial surfaces, Agricultural areas, and Scrub/ Herbaceous vegetation exhibit a positive rate of change, while the categories Forest and Open spaces with little or no vegetation display a decreasing trend. Consequently, the areas of patches and perforated have expanded in terms of area units, contributing to a reduction in forested areas (Core 3) due to fragmentation. As a result, forested areas smaller than 500 acres (Core 1 and 2) have increased. Finally, our research provides a methodological framework for image classification and assessment of landscape change and fragmentation, crucial information for decision makers in a current agricultural zone of northwestern Peru.

1. Introduction

On a global scale, in the last 25 years, almost 125 million hectares of forest have been deforested (Curtis et al., 2018), and a current global rate of forest loss of 0.6% per year (Hansen et al., 2013), likewise, for the period 1990 to 2015, the total forest area of the world decreased by 3% (Ban et al., 2019). Specifically, South America, between 2015 and 2020 lost >15 million hectares of forest, becoming the second most deforested region in the world, with agriculture, forestry, forest fires and urbanization being the main drivers of deforestation (Chamberlain et al., 2020;

* Corresponding author at: Instituto de Investigación para el Desarrollo Sustentable de Ceja de Selva (INDES-CES), National University Toribio Rodríguez de Mendoza (UNTRM), Chachapoyas 01001, Peru.
E-mail addresses: darwin.gomez@untrm.edu.pe (D. Gómez-Fernández), rsalas@indes-ces.edu.pe (R.S. López), jhon.zabaleta@untrm.edu.pe (J.A. Zabaleta-Santisteban), angel.medina@untrm.edu.pe (A.J. Medina-Medina), malluri.gonas@untrm.edu.pe (M. Goñas), jhonsy.silva@untrm.edu.pe (J.O. Silva-López), soliva@indes-ces.edu.pe (M. Oliva-Cruz), nrojasb@unam.edu.pe (N.B. Rojas-Briceño).

https://doi.org/10.1016/j.ecoinf.2024.102738
Received 22 October 2023; Received in revised form 21 July 2024; Accepted 22 July 2024
Available online 28 July 2024

Curtis et al., 2018).

Forest fragmentation refers to changes in forest cover and can be measured using land cover maps derived from satellite products (Myroniuk et al., 2020). Anthropogenic activities, such as agricultural expansion and urbanization(Ellis and Ramankutty, 2008), as well as logging and stand burning (Haddad et al., 2015), are the main causes of forest landscape loss and fragmentation (Negi et al., 2019). Under the dual actions of climate change and land cover change, global biodiversity and ecosystem functioning face serious threats, especially in globally recognized biodiversity hotspots (DeFries et al., 2002; Kanade and John, 2018).

Forests are a crucial terrestrial ecosystem, and have an indispensable role in nutrient cycling and energy flow in ecological processes (Chazdon et al., 2016). Fragmentation of landscapes results in a mixture of land cover patches of different classes, sizes and shapes (Numata et al., 2011). Thus, forest landscape fragmentation can negatively affect many processes that occur within an ecosystem (Xun et al., 2014), in addition, fragmentation impacts species richness and distribution patterns of biodiversity (Gibson et al., 2013; Pardini et al., 2010), ecosystem services (Nagendra et al., 2009; Rocha-Santos et al., 2016; Uddin et al., 2015), habitat quality (Fahrig, 2003; Reddy et al., 2013), and invasive species emergence (Reddy et al., 2013; Thuiller et al., 2008).

Specifically, the loss and fragmentation of forest cover is considered the main cause of global ecosystem degradation (Newman et al., 2014). In addition, fragmented forests may be more vulnerable to stress and have lower resilience compared to connected forests (Shimizu et al., 2017). Specifically, the higher the degree of landscape fragmentation, the lower its stability, due to the reduction of resources and therefore, the survival of key species of the ecosystem is put at risk (Zhang et al., 2021). Therefore, quantifying landscape changes is imperative to understand the spatial and structural viability of land use and its associated ecological effects (Turner, 2005).

A recent study revealed that 70% of the world's forests are within 1 km of the forest edge, subject to the degrading effects of fragmentation (Ganivet and Bloomberg, 2019). Frequent landscape fragmentation occurs particularly in many developing countries (Abdullah et al., 2019). Thus, there has been a growing need to better understand the importance of landscape fragmentation processes (Hermosilla et al., 2019; Hysa and Başkaya, 2017).

The level of landscape fragmentation is an important attribute of land pattern because it has potential implications for land loss prevention and management [30]. That is, it can change environmental conditions and species composition in ways that could influence forest susceptibility (Schwartz et al., 2019). Thus, assessing the extent of fragmented forests can help inform policy and decision making for forest management practices (Wulder et al., 2009). Therefore, forest mapping on fragmented landscapes is essential at a regional scale (Myroniuk et al., 2020).

Additionally, studies have been conducted examining forest fragmentation in different regions of the world. For example, in Bangladesh, between 1989 and 2021, using remote sensing data, identified changes in forest cover and forest fragmentation, highlighting the importance of forest restoration (Hassan et al., 2023). Another study optimized the VOR model to measure ecosystem health using remote sensing technology, showing a gradual decline in regional ecosystem health over time (Bao et al., 2022). Similarly, a study analyzed the impact of landscape fragmentation on the provision of ecosystem services over three decades, identifying a negative relationship between landscape fragmentation and the value of these services (Do et al., 2022).

By 2030, it is estimated that the Peruvian Amazon will experience greater deforestation and forest degradation than any other region, driven by agriculture, commercial mining, and land artificialization due to urbanization (Smith and Schwartz, 2015). To date, studies in the Amazonas region have focused on LULC changes; however, landscape fragmentation levels have been scarcely studied (Rojas Briceño et al., 2019). Therefore, it is essential to provide a methodological framework that integrates the assessment of LULC changes and associated fragmentation in high Andean areas, where the expansion of agriculture and forest resource utilization continues to advance.

Landsat images are considered the standard Earth observation data for large-scale ecological monitoring and provide unique opportunities to assess changes in forest cover (Wulder et al., 2012), due to their long time series, high spatial resolution and free access (Huang et al., 2010; Shen et al., 2019; Zhu and Woodcock, 2014). In recent decades, satellite imagery collected by Landsat platforms in forestry applications has increased due to the availability of long time series of satellite observations of land cover and its dynamics (Gu et al., 2020). Also, many studies have detected changes in forest cover and monitored forest fragmentation using remote sensing data at regional and global scales (Da Ponte et al., 2017; Gong et al., 2013; Vogeler et al., 2020).

On the other hand, the advent of cloud-based computing Google Earth Engine (GEE) (Gorelick et al., 2017), in recent years has helped to facilitate large-scale studies using high-performance mapping algorithms (Garcia et al., 2023; Kennedy et al., 2018; Parente and Ferreira, 2018; Zhu et al., 2019). Thus, GEE with its robust computation and storage capabilities, has attracted a great deal of attention (Gorelick et al., 2017) and has been widely applied in vegetation monitoring (Wang et al., 2019a; Xie et al., 2019), crop mapping (Jin-Ming et al., 2019; Wang et al., 2019b), and LULC classification (Ge et al., 2019; Tsai et al., 2019). Also, GEE allows easy access to different publicly available datasets, including the collection of preprocessed Landsat imagery, reducing the time needed to generate accurate maps (Myroniuk et al., 2020). In particular, Landsat data hosted on the GEE platform provide a unique opportunity to monitor forest cover change at high spatial resolutions, from local to global scales.

Therefore, we used Landsat satellite products and GIS tools to evaluate forest landscape fragmentation in Northwest Peru. To do this: i) in GEE we obtained accurate LULC maps for the years 1989, 2005 and 2023, ii) we analyzed the changes and level of fragmentation for each period using Landscape Fragmentation Tool v2 in ArcGIS software. Finally, this study provides baseline information on the current state of landscape conservation for proper land management. This evaluation strategy will allow not only quantifying landscape fragmentation but also providing valuable information for decision-making in environmental management and conservation of natural resources in the region.

2. Materials and methods

2.1. Study area

The study area extends from 78°06′ to 78°58′ west longitude, and 5°30′ to 6°02′ south latitude, covering 2904.96 km2, has elevations from 351 to 3684 m.a.s.l. and encompasses the Alto Marañón II and III interbasins, as well as the lower Utcubamba river basin, as shown in Fig. 1.

This area was chosen as a case study because it is currently the most affected sector by the cultivation of rice, coffee, cocoa, and extensive livestock farming in the aforementioned watersheds of the Amazonas and Cajamarca regions, located in the northwest Peru (Gobierno Regional de Amazonas (GOREA) and Instituto de Investigaciones de la Amazonía Peruana (IIAP), 2007; Gobierno Regional de Cajamarca (GRC), 2010MIDAGRI, 2021).

On the other hand, according to the climatic classification elaborated by SENAMHI (2020), the study area is conditioned by the C(*r*)B type, that is, Semi-dry with abundant humidity in all seasons of the year, and with temperate temperature efficiency, the maximum temperature ranges from 21 to 25 °C, and minimum from 7 to 11 °C, with respect to precipitation, in this type of climate 700 to 2000 mm per year are registered.

2.2. Methodological flow

Fig. 2 presents an overview of the methodological flow employed for

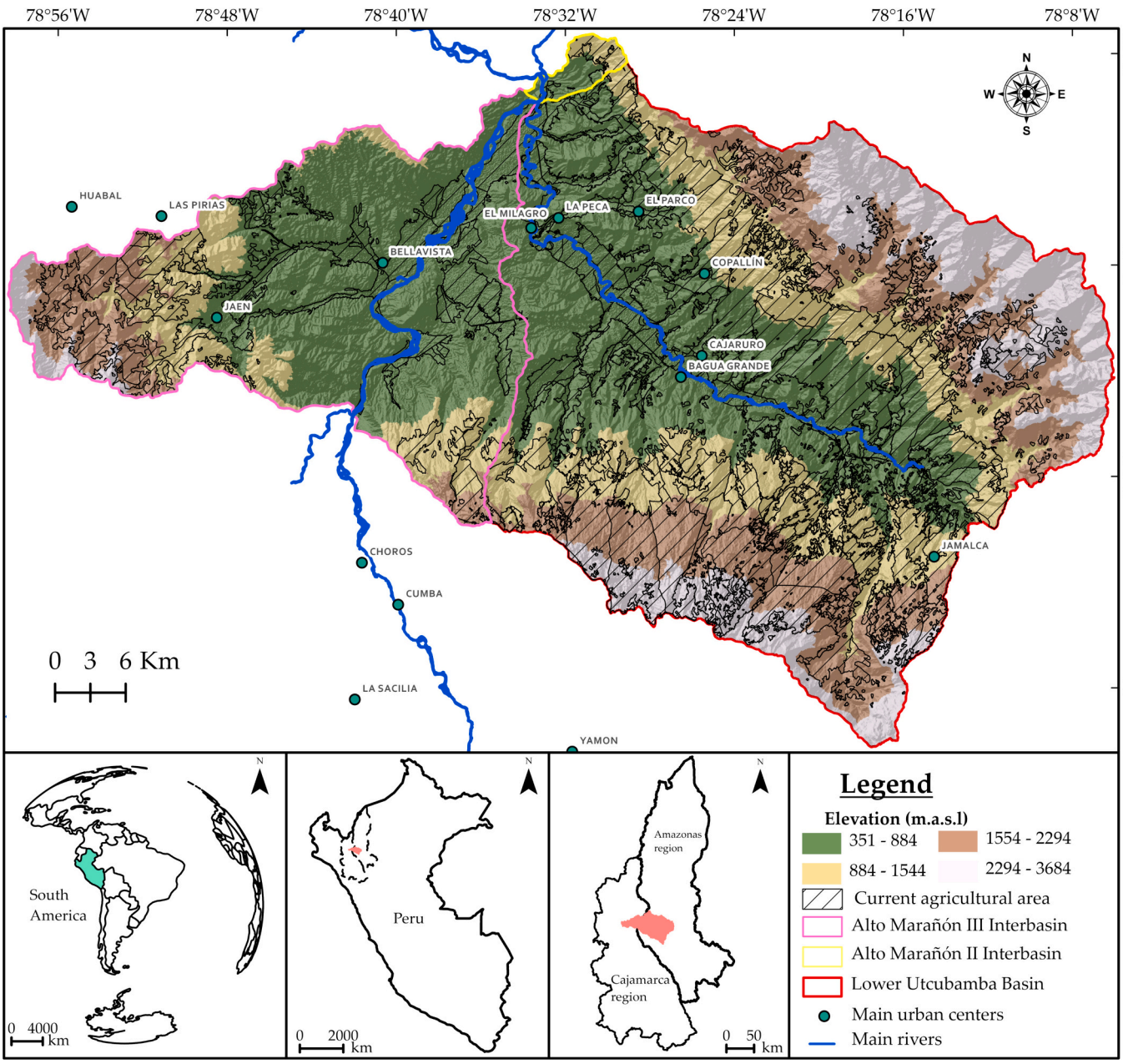

Fig. 1. Geographic location of study area in Northwest Peru.

the analysis of landscape fragmentation in Northwest Peru since 1989 to 2023, applying Landscape Fragmentation Tool (LFT) as GIS tools and Landsat image classification.

We initiated the process of identifying the optimal combination of data to effectively classify Landsat 8 images. To achieve this, within the GEE platform, we filtered the image collection removing cloudy areas using a cloud mask, then, we combined spectral bands, indices of vegetation, soil, water, and clusters generated, this process yielded a total of 31 unique data combinations.

We used the Random Forest algorithm for classification, using training points for each data set. Subsequently, an evaluation was performed using field points to determine the accuracies of the 31 data sets. An ANOVA was then used to identify significant differences between the data sets. Once the combination yielding the highest accuracies was identified, the 1989 and 2005 maps were ranked using the input data from the most accurate dataset. These maps were then reclassified into forest and non-forest categories. Finally, fragmentation maps were generated for all three years using ArcMap 10.5 and LFT v2.

2.3. Obtaining LULC maps in GEE

2.3.1. Data source and classification algorithm

LULC maps were generated in GEE (Gorelick et al., 2017), from the oldest year with adequate data (1989 in our case) to the most recent year (2023), divided into two periods with similar number of years (1989 to 2005 and 2005 to 2023). For this purpose, we use Landsat images (Landsat 4, 5 y 8 images courtesy of the U.S. Geological Survey). The data from the Landsat-4 Thematic Mapper (TM) mission were used to obtain the 1989 LULC map, whereas Landsat-5 TM images were employed for the 2005 LULC map, and finally, Landsat-8 Operational Land Imager and Thermal Infrared Sensor (OLI-TIRS) images were used to obtain the 2023 LULC map.

The Landsat data used for the three years of analysis were from Level 2, Collection 2, Tier 1, this means that the surface reflectance was

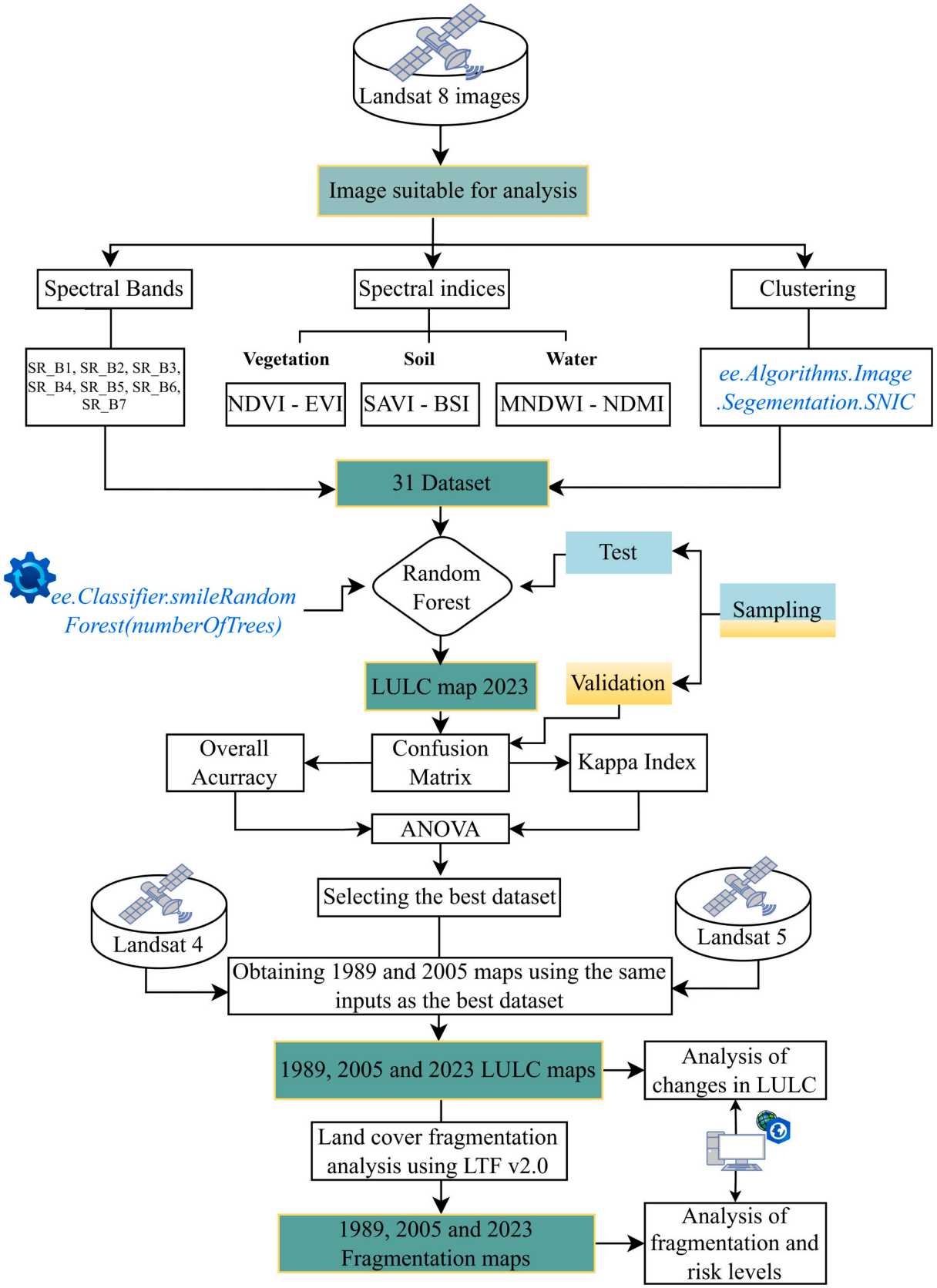

Fig. 2. Methodological flow used in the analysis of landscape fragmentation in Northwest Peru from 1989 to 2023.

atmospherically corrected using the Land Surface Reflectance Code; this correction eliminated the influence of aerosol scattering, thin clouds, and other atmospheric effects on the detection and characterization of land surface changes (Masek et al., 2006; Vermote et al., 2016). Additionally, to avoid problems associated with cloud cover, a cloud mask procedure was conducted using the quality assessment band available in the Landsat data. We used Bitmasks 1, 2, 3, 4, and 6, which represent dilated clouds, high confidence cirrus, clouds, cloud shadows, and clear conditions, respectively. For more details, refer to Section 1 of the script shared in the supplementary material.

On the other hand, based on the fact that, with respect to other classification algorithms running in GEE, Random Forest (RF) is one of the machine learning classifiers with the best accuracies in the classification of satellite images to obtain LULC maps (Gómez Fernández et al., 2022; Ouma et al., 2022; Shetty, 2019; Talukdar et al., 2020), therefore, for the classification, the RF algorithm was trained using training points collected in the field and the inputs of the best dataset, obtaining LULC maps with 30-m pixels, according to the spatial resolution of Landsat missions, finally, through a post classification and visual inspection, the products were improved.

2.3.2. Datasets of classification variables

A total of 31 data combinations were generated (Table 2), resulting from the combination of spectral bands, vegetation indices, soil, water, and clusters. Subsequently, the best dataset was selected as the combination that accumulated the highest overall accuracy by summing the accuracies of the 9 decision trees. To determine the optimal number of decision trees, the accuracies of the 31 datasets were summed, and the decision tree with the highest overall accuracy accumulated was chosen.

The input data were ***i)*** spectral bands: Ultra blue, Blue, Green, Red, Near Infrared (NIR), Shortwave Infrared 1 (SWIR-1) and Shortwave Infrared 2 (SWIR-2), ***ii)*** Vegetation Indices: Normalized Difference Vegetation Index (NDVI) and Enhanced vegetation index (EVI), ***iii)*** Soil Indices: Soil Adjusted Vegetation Index (SAVI) and Bare Soil Index (BSI), ***iv)*** Water Indices: Modified Normalized Difference Water Index (MNDWI) and Normalized Difference Moisture Index (NDMI), and ***v)*** Clusters.

The aforementioned spectral indices were calculated according to the formulas in Table 1. In order to obtain clusters, a superpixel clustering based on Simple Non-Iterative Clustering (SNIC), was performed in GEE using the function ee.Algorithms.Image.Segmentation.SNIC. For more details, refer to Section 2 of the script shared in the supplementary material.

Table 2 shows the obtained combinations of spectral bands, vegetation, soil, water indices, and clusters. The combinations were generated online (https://es.planetcalc.com/3757/), and to obtain the 31 datasets, combinations of size one, two, three, four, and five were used.

2.3.3. Definition of LULC classes

The LULC classes defined in this research were aligned with the Coordination of Information on the Environment (CORINE) Land Cover (CLC) methodology. Table 3 below shows the LULC classes present in the study area and their respective descriptions.

Table 2
Datasets obtained.

Name	Inputs	Name	Inputs
Dataset 1	Spectral bands (B)	Dataset 17	B + VI + WI
Dataset 2	Vegetation Indices (VI)	Dataset 18	B + VI + C
Dataset 3	Soil Indices (SI)	Dataset 19	B + SI + WI
Dataset 4	Water Indices (WI)	Dataset 20	B + SI + C
Dataset 5	Cluster (C)	Dataset 21	B + WI + C
Dataset 6	B + VI	Dataset 22	VI + SI + WI
Dataset 7	B + SI	Dataset 23	VI + SI + C
Dataset 8	B + WI	Dataset 24	VI + WI + C
Dataset 9	B + C	Dataset 25	SI + WI + C
Dataset 10	VI + SI	Dataset 26	B + VI + SI + WI
Dataset 11	VI + WI	Dataset 27	B + VI + SI + C
Dataset 12	VI + C	Dataset 28	B + VI + WI + C
Dataset 13	SI + WI	Dataset 29	B + SI + WI + C
Dataset 14	SI + C	Dataset 30	VI + SI + WI + C
Dataset 15	WI + C	Dataset 31	B + VI + SI + WI + C
Dataset 16	B + VI + SI		

Table 3
LULC classes based on CLC methodology.

Class	Description	Code	RGB color
Artificial surfaces	All classes of continuous and discontinuous urban fabric.	1	230–000-077
Agricultural areas	All arable land, permanent crops, pastures and heterogenous agricultural areas.	2	255–255-168
Forest	All broad-leaved, coniferous and mixed forest	3	128–255-000
Scrub and/or herbaceous vegetation	All natural grasslands, Moors and heathland, Sclerophyllous vegetation and Transitional woodland-shrub	4	204–242-077
Open spaces with little or no vegetation	All sand, bare rocks, sparsely vegetated and burnt areas	5	230–230-230
Water bodies	All water courses and water bodies	6	128–242-230
No data	No data	999	–

2.3.4. Sampling size and validation areas

On this occasion, to define the training and testing samples, we relied on Chuvieco (2020), who argues that for categorical variables, at least 196 test points should be considered. Furthermore, Chuvieco (2020), also mentions that, at times, this number can be very small when compared to the total number of pixels in the image. Therefore, we explored new sampling strategies that combine the previous scientific foundation with the current capabilities of GEE.

Taking into account Congalton (1991) and Hay (1979), who suggest at least 50 pixels per thematic class, we decided to implement an alternative strategy. Instead of strictly distributing 196 training areas among the 6 thematic classes, we chose to include pure training areas. These well-identified areas should contain at least 50 pixels in total and prominently represent the class of interest. This distribution was carried out through simplified random sampling (Chuvieco, 2020), allowing us to effectively capture variability within each class and improve the

Table 1
Spectral indices calculated for each collection.

Index	Formula	Reference
NDVI	$(NIR - RED)/(NIR + RED)$	(Rouse et al., 1974)
EVI	$C^*[(NIR - RED)/(NIR + C1^*RED - C2^*BLUE + L)]$	(Gao et al., 2003)
SAVI	$[(NIR - RED)/(NIR + RED + L)]^*1 + L$	(Huete, 1988)
BSI	$[(RED + SWIR) - (NIR + BLUE)]/[(RED + SWIR) + (NIR + BLUE)]$	(Rikimaru et al., 2002)
MNDWI	$(GREEN - SWIR1)/(GREEN + SWIR1)$	(McFeeters, 2007)
NDMI	$(NIR - SWIR1)/(NIR + SWIR1)$	(Wilson and Sader, 2002)

*Where: C = 2.5; C1 = 6; C2 = 7.5; L = 0.5 and Blue, Red, Green, NIR, SWIR depend on each Landsat. Mission band.

representativeness of our samples.

Finally, for the validation areas, a minimum of 25% of the training areas was considered. Therefore, in this research, we used 40 training areas, comprising 2463 pixels, and, additionally, 10 validation areas, comprising 866 pixels. For more details, please refer to Section 3.1 of the script shared in the supplementary material.

2.3.5. Measuring the accuracy of LULC maps

The assessment of accuracy can be approached from various perspectives, utilizing expert judgment (visual inspection) or external statistical sources, and this process must be carried out to ensure the highest reliability of the results with the ground truth (Blissag et al., 2024). In this research, the measurement of accuracy was based on the validation points. Using this approach, the confusion matrix was calculated, allowing us to obtain the Overall Accuracy (OA) and Kappa Index (KI), coefficients necessary for the evaluation of classification accuracy (Thomlinson et al., 1999). For this purpose, Eqs. (1) and (2) were followed.

$$OA = \frac{Total\ number\ of\ pixel\ classified\ correctly}{total\ number\ of\ pixels} * 100 \quad (1)$$

$$KI = \frac{N\sum_{i=1}^{n} a_{i,i} - \sum_{i=1}^{n}(T_i + F_i)}{N^2 - \sum_{i=1}^{n}(T_i + F_i)} \quad (2)$$

Where: i represent the class number. N is the total number of classified values compared to truth-values. $a_{i,i}$ is the number of values of the truth class i classified also as class i, which is the values found along the diagonal of the confusion matrix. F_i represents the total number of predicted values of the i class and T_i is the total number of truth-values of the i class (Foody, 2020; Stehman, 1997a; Stehman, 1997b).

Additionally, to make a decision based on the two-accuracy metrics, Table 4 shows the classification accuracy according to the Kappa index, and the operator's decision on the classification.

Finally, in order to select a specific dataset, an ANOVA of one way of the 31 datasets was performed in Google Colaboratory, considering a significance level of 95%. The null hypothesis was that "all the means of the dataset accuracies are equal," while the alternative hypothesis was that "at least one mean is different from the others". This analysis was conducted in relation to the number of repetitions, taking into account each accuracy obtained with different numbers of decision trees.

2.4. Measurement of LULC change

We calculated the areas (in km^2) of each LULC class for the years 1989, 2005, and 2023. This enabled us to ascertain the gains and losses of each category over the evaluated years. Subsequently, we determined the rate of change using Eq. (3), as described in (Food and Agriculture Organization of the United Nations, 1993; Puyravaud, 2003).

$$r = \left(\frac{1}{t2 - t1}\right) * ln\left(\frac{A2}{A1}\right) \quad (3)$$

Where: r is the rate of change per year, t represents year and A the area covered by the class, subscripts 2 and 1 represent the final and initial period, respectively.

Table 4
Classification accuracy according kappa index.

Kappa Index	Accuracy	Decision
> 0.90	Very high	Acceptable
0.80–0.90	High	Acceptable
0.60–0.79	Moderate	Depend of application
< 0.50	Low	Not acceptable

Note: Table data adapted from (Cohen, 1960; Landis and Koch, 1977).

2.5. Fragmentation measurement

In the ArcGIS 10.5 software, the Landscape Fragmentation Tool (LFT) (Uddin et al., 2015; Vogt et al., 2006), was utilized to generate fragmentation maps. Initially, the LULC maps were converted into a binary format (foreground/background). The Forest and Scrub/Herbaceous vegetation classes were designated as the foreground, while the remaining classes (Artificial surfaces, Agricultural areas, Open spaces with little or no vegetation and Water bodies) comprised the background.

As for the input parameters of the LFT, the reclassified raster was assigned two classes: 1 = nonforest (background), and 2 = forest (foreground), ultimately with an edge width of 100 m, as argued by Uddin et al. (2015) and Vogt et al. (2006). The fragmentation maps generated had the following forest patterns and/or fragmentation categories: The "Core" is situated at a considerable distance from the boundary between forest and non-forest areas, while the "Patch" consists of cohesive forest regions that are too limited in size to encompass the core forest. The "Perforated" establishes the limits between the core forest and relatively small perforations, and the "Edge" encompasses interior boundaries with relatively large perforations, as well as the external boundaries of core forest regions (Vogt et al., 2006).

2.5.1. Determination of transitions and risk levels

Due to fragmentation causing a loss of connectivity within the ecosystem, it's considered one of the main drivers of landscape degradation (Jaramillo et al., 2023), by intersecting and summing the codes of fragmentation categories for the years 1989, 2005, and 2023, in ArcGIS Pro version 3.0.1, we generated transition matrices for the periods 1989–2005, 2005–2023 and 1989–2023.

In Table 5, we present the base transition matrix, with the 6 categories of fragmentation, this allowed us to identify the changes from one category to another in the aforementioned periods.

On the other hand, in Table 6 shows the risk levels that each transition represents, based on the definitions of each forest pattern (Vogt et al., 2006).

3. Results

3.1. Dataset accuracy metrics

We obtained 31 datasets and calculated their OA and KI. In Fig. 3 displays the variation of OA and KI along the Y-axis, corresponding to the number of decision trees on the X-axis.

It can be observed that OA and KI exhibit an increasing trend up to a certain point. Afterward, they stabilize or begin to decrease. This phenomenon is associated with the number of decision trees utilized. In some dataset increasing the number of decision trees contributes to enhanced accuracies, while in others, the opposite occurs. The accuracies of the 31 datasets were highly variable, in the case of OA, it ranged from 0.33 to 0.92, while KI varied between 0.2 and 0.90.

Five datasets were identified that exceeded 0.9 for overall accuracy and 0.87 for Kappa index, of which Dataset 19 was selected as the most suitable due to its highest cumulative OA value. Fig. 4 shows the cumulative overall accuracy of the 31 datasets as a function of the 9 types of decision trees used, identifying Dataset 19 as the best dataset with 8.32 and 0.92 for cumulative and average OA, respectively.

Fig. 4 confirms the positive impact of spectral indices on classification accuracy. For example, in Dataset 1, which only utilized spectral bands, an acceptable accuracy was achieved. However, by adding water indices, this accuracy slightly improved, and by also including soil indices, the highest classification accuracy was reached, as observed in the stacked bar of Dataset 19. On the other hand, a noticeable aspect is the low accuracy of Dataset 5, which only used the cluster band. This low accuracy negatively affected the accuracy of datasets that included this band. Therefore, caution is recommended when combining it for a

Table 5
Transition matrix of fragmentation categories.

			Year 2					
	Categories		Patch	Edge	Perforated	Core 1	Core 2	Core 3
		Code	1	2	3	4	5	6
Year 1	Patch	10	11	12	13	14	15	16
	Edge	20	21	22	23	24	25	26
	Perforated	30	31	32	33	34	35	36
	Core 1 (<250 acres)	40	41	42	43	44	45	46
	Core 2 (250–500 acres)	50	51	52	53	54	55	56
	Core 3 (>500 acres)	60	61	62	63	64	65	66

Table 6
Considered transitions and risk levels.

Color	Description	Risk level	Risk code
	Patches unchanged.	High Risk	****
	Core 1, 2, or 3 to Patches and Edges.	High Risk	****
	Edge to Patch and Perforated to Patch and/or Edge.	High Risk	****
	Edge unchanged.	Medium Risk	***
	Perforated unchanged.	Medium Risk	***
	Patch to Edge and/or Perforated and Edge to Perforated.	Medium Risk	***
	Core 1, 2, or 3 to Perforated.	Medium Risk	***
	Core 1 unchanged.	Moderate Risk	**
	Patches and edges to Core 1, 2, or 3.	Moderate Risk	**
	Perforated to Core 1, 2, or 3.	Moderate Risk	**
	Core 2 to Core 1 and Core 3 to Core 1 or 2.	Moderate Risk	**
	Core 2 unchanged.	Low Risk	*
	Core 3 unchanged.	Low Risk	*
	Core 1 to Core 2 and Core 1, 2 to Core 3.	Low Risk	*

definitive classification.

Therefore, to solidify the results and demonstrate significant differences among the datasets, the results of the ANOVA conducted are shown in Table 7.

Table 7 displays the principal results of ANOVA, indicating a highly significant *p*-value, which is less than the conventional significance level of 0.05, additionally, F-statistic is greater than the critical value (0.05). Therefore, there is compelling evidence to reject the null hypothesis that the average of overall accuracy and kappa index of all datasets are equal. Instead, we accept the alternative hypothesis, suggesting that at least one average of OA and KI among the datasets differs from the others.

For more details regarding the global accuracy, Fig. 5 illustrates the differences and similarities between groups derived from the Tukey Honestly Significant Difference (HSD) test, considering a Family-Wise Error Rate (FWER) of 0.05 to control the overall risk of type I error in the statistical analysis. In 69% of the comparisons, there are significant differences, meaning that the means of OA aren't equal. On the other hand, in the remaining 31%, statistically the means of global accuracies are equal, as depicted in Fig. 5, where the blue color indicates similarity between means and gray the opposite.

Then, after selecting the best dataset, we proceeded to identify the most effective decision tree. On this occasion, in sub-Fig. 6a, the cumulative and average overall accuracy of each decision tree is presented, and in sub-Fig. 6b, the same overall accuracy but standardized. This standardization was carried out because the differences between the trees were minimal and not clearly appreciated in sub-Fig. 6a.

As seen in Fig. 6, there aren't differences in the cumulative overall accuracies, which was also statistically confirmed, obtaining a p-value of 0.99 in an ANOVA performed. Therefore, with the parameters considered in this research, the number of decision trees doesn't directly influence the overall accuracy of the classification. However, it is noteworthy that when 100 decision trees were used, the overall accuracy was slightly higher than the others.

Additionally, Fig. 7 shows the distribution of the overall accuracies of the 9 decision trees, indicating that the highest density of cases is concentrated in the accuracy range between 0.6 and 1. This suggests a common trend towards high levels of overall accuracy in the classifications performed by all types of trees.

3.2. LULC maps

As Dataset 19 obtained higher accuracies, its inputs were used to obtain the LULC map of 1989 and 2005, and 100 decision trees for each year. Fig. 8 displays the RGB and LULC maps for 1989, 2005, and 2023.

3.2.1. LULC changes

Fig. 9 shows the square kilometers covered by the different LULC categories and Table 8 shows gains and losses for the three years of analysis.

From Fig. 9 and Table 8, a shift towards more intensive land use and a loss of forested areas is evident. Over the analyzed periods, there is an acceleration in the conversion of land to agricultural and urban uses at the expense of natural and semi-natural areas, reflecting a clear pattern of urbanization and expansion of agricultural areas.

Between 1989 and 2005, artificial surfaces increased from 16.2 km^2 to 33.4 km^2, following the same trend as agricultural areas, which rose from 571.2 km^2 to 676.5 km^2. Conversely, forest cover decreased from 556.2 km^2 to 470.36 km^2, as did open spaces with little or no vegetation, which shrank from 973.9 km^2 to 796.9 km^2.

From 2005 to 2023, artificial areas continued to expand, reaching 44

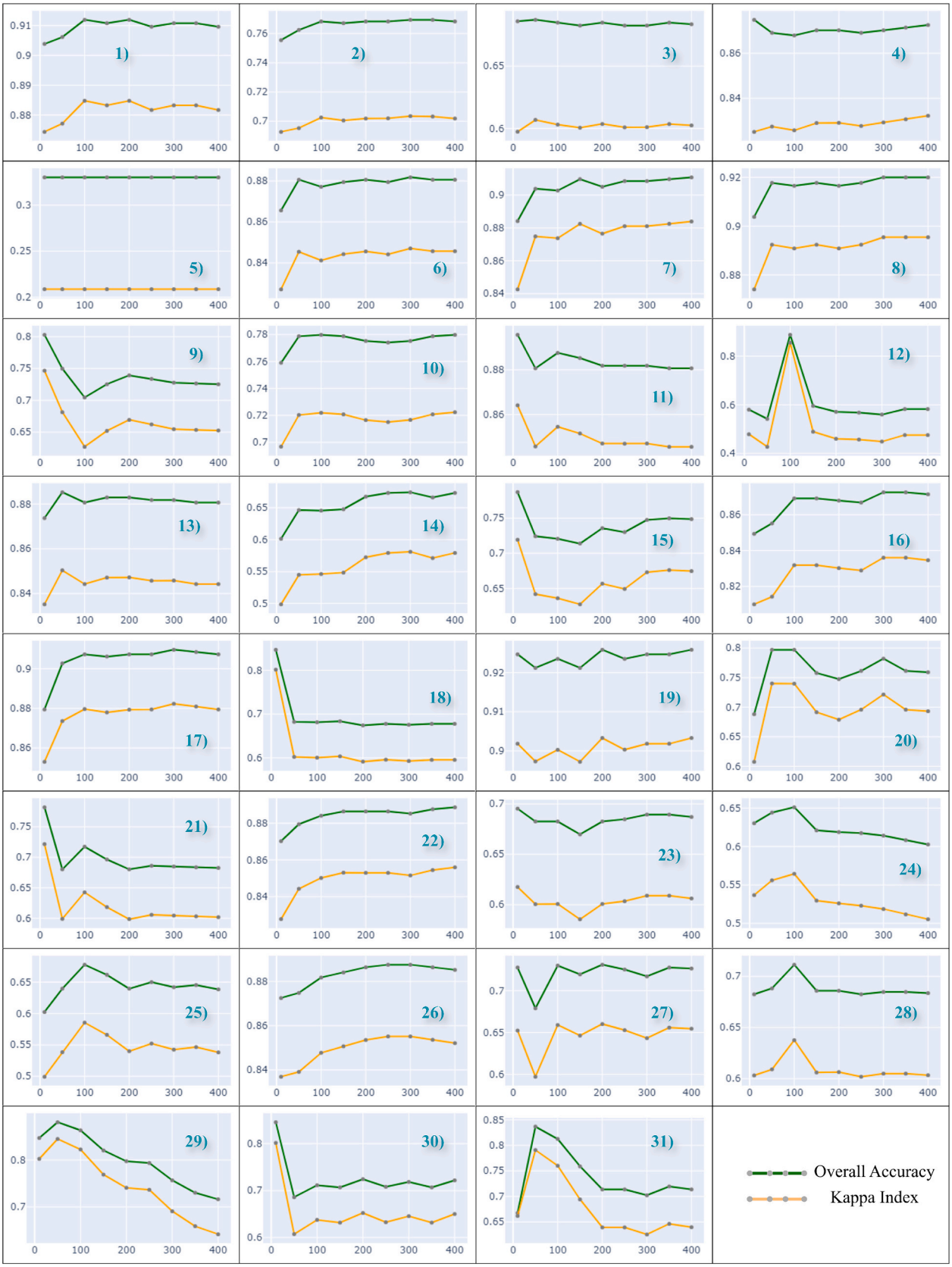

Fig. 3. Variation of OA and KI among the 31-dataset obtained for 2023, as influenced by the number of decision trees utilized.

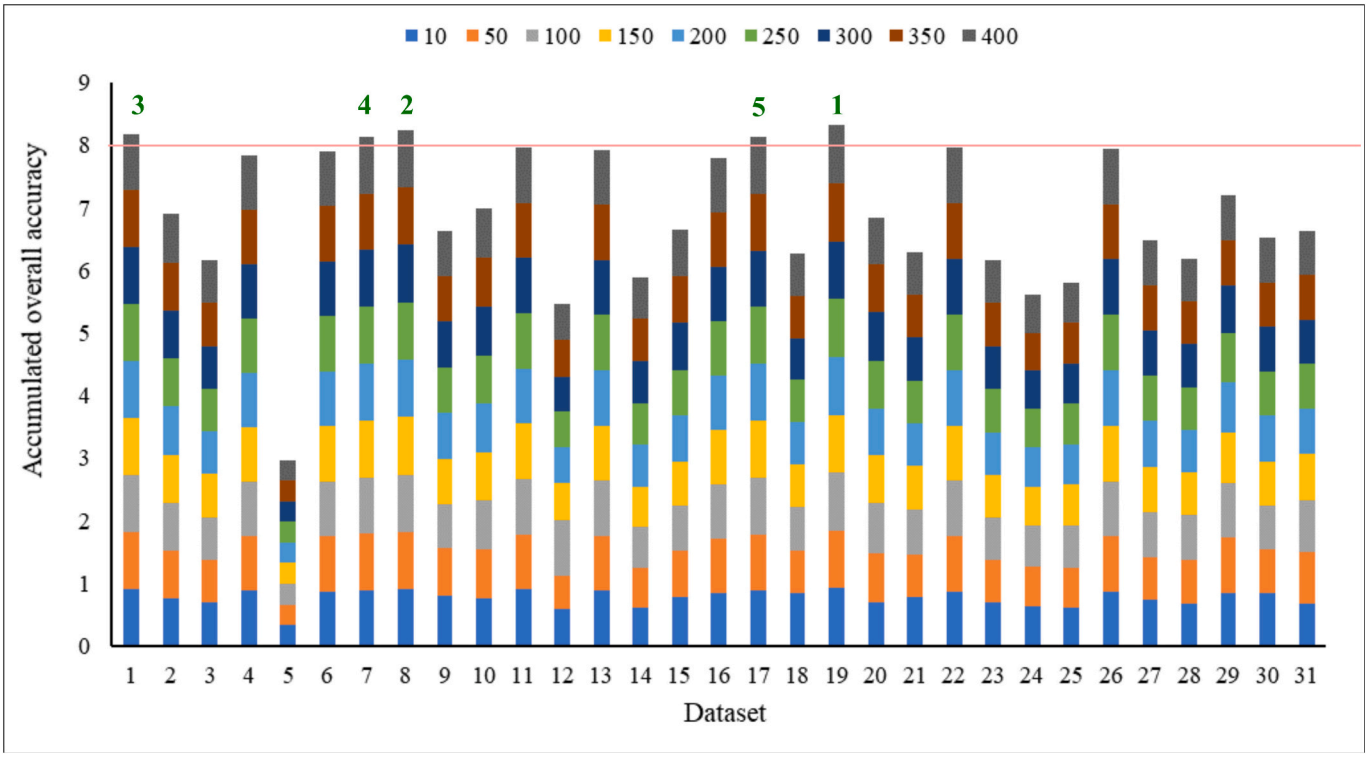

Fig. 4. Variation of the cumulative overall accuracy of the 31 datasets according to the 9 types of decision trees considered.

Table 7
Summary of the analysis of variance performed.

	F-Statistic	*P*-value
Overall accuracy	161.36	$5.14e^{-145}$
Kappa index	158.93	$3.06e^{-144}$

km^2, and agricultural areas grew to 954.2 km^2. Forest cover continued to decline to 410 km^2, and open spaces with little or no vegetation also decreased to 526.56 km^2.

Overall, from 1989 to 2023, artificial surfaces increased by 27.80 km^2, while agricultural areas expanded by 383.00 km^2. The accumulated loss of forest cover was 145.70 km^2, and open spaces with little or no vegetation decreased by 447.34 km^2.

While Table 8 provides substantial information, Table 9 below shows the rate of change for the periods 1989–2005, 2005–2023 and 1989–2023.

As shown in Table 9, artificial surfaces grew at an annual rate of 2.94%, and agricultural areas at a rate of 1.51% per year. Forest cover decreased at an annual rate of −0.89%, while shrub and/or herbaceous vegetation grew at a rate of 0.71% per year. Open spaces with little or no vegetation decreased at a rate of −1.81% per year, and water bodies increased at an annual rate of 0.49%. These trends confirm the ongoing

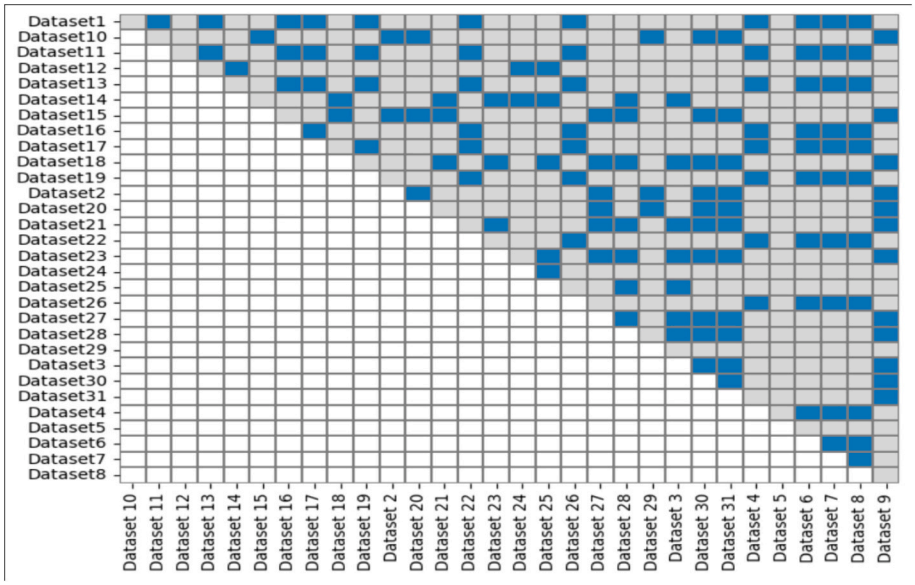

Fig. 5. Differences and similarities between groups considering OA values.

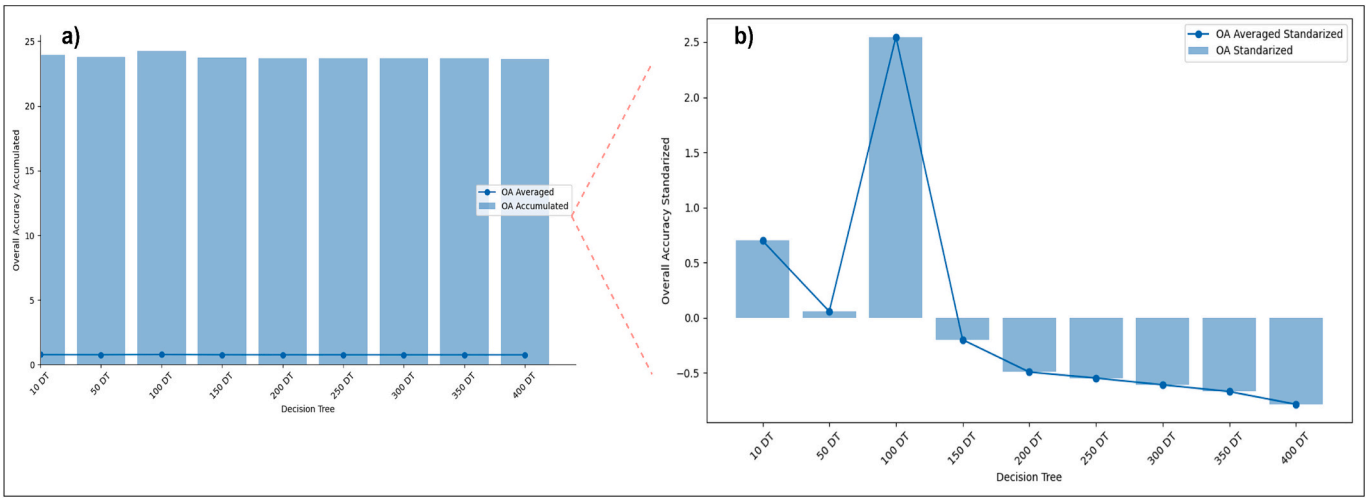

Fig. 6. Cumulative and average overall accuracy (a) and its standardization (b) of the 31 datasets based on each decision tree used.

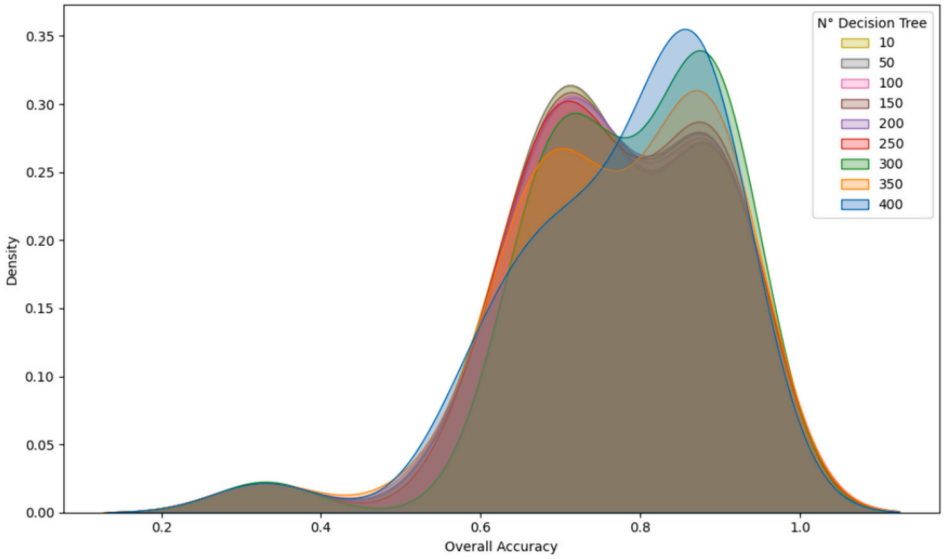

Fig. 7. Distribution of the overall accuracy of the 31 datasets based on each decision tree used.

urbanization and agricultural expansion over time, as well as the continuous decrease in forests and open spaces.

3.3. Fragmentation maps

Fig. 10 shows the fragmentation levels for the years 1989, 2005 and 2023. It can be seen that in 1989 the study area presented a greater forest core, while in 2023 the appearance of patches and edges is more frequent.

From Fig. 10 it can be inferred that the area covered by patches has increased, as have the edges, which is not the case for fragmentation category Core 3 (Cores >500 acres). For this reason, Fig. 11 shows the area covered calculated in km^2 of the different fragmentation categories, showing that, effectively since 1989 to 2023, patches increased 21.81 km^2, and edges increased 156.95 km^2, while Core 3 has a decreasing trend, losing a total of 322.24 km^2 for the period of analysis, affecting the increase of Core 1 (Cores <250 acres), which increased 49.95 km^2.

In summary, Figs. 10 and 11 show that the appearance of patches and edges (as a result of agricultural activities or other factors) has brought with it the fragmentation of forests, that is, the increase of level 1 and 2 cores.

Below, Fig. 12 displays the transitions of fragmentation categories for the periods 1989–2005, 2005–2023, and 1989–2023. Additionally, Table 8 provides detailed information on the risk levels and the covered area (km^2) for each transition.

Table 10 consolidates the changes in the four risk levels for the three analysis periods, showing a trend towards increased fragmentation and a decrease in core forest areas. Specifically, from 1989 to 2005, the transition from Core to Patch-Edge covered an area of 71.96 km^2, representing 66.76% of the total high-risk transitions, and increased to 86.93 km^2 by 2023. Similarly, the transition from Edge to Patch and from Perforated to Patch covered 28.75 km^2 in the first period and increased to 41.92 km^2 by 2023.

Regarding medium-risk transitions, the transition from Core to Perforated covered an area of 132.34 km^2 (44.48%) from 1989 to 2005 but decreased to 118.50 km^2 by 2023. On the other hand, moderate-risk transitions showed more stable patterns. For example, the transitions from Perforated to Cores covered 35.12 km^2 from 1989 to 2005, then increased to 75.54 km^2 by 2023, highlighting a trend towards the consolidation of fragmented areas.

Finally, low-risk transitions showed minimal changes. Transitions of the Core 3 unchanged covered the largest area within this level,

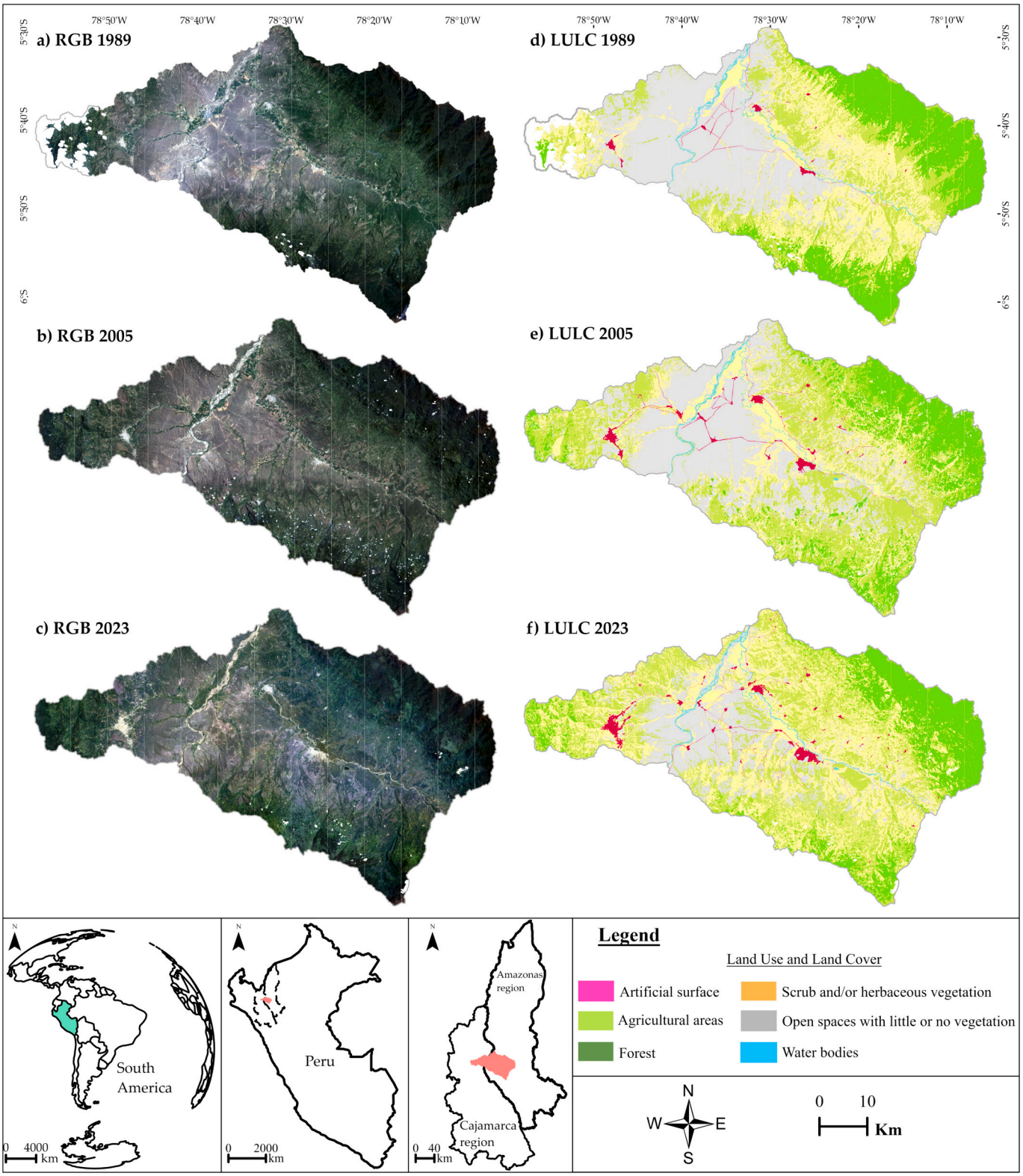

Fig. 8. RGB Compositions and LULC maps obtained for 1989, 2005 and 2023. In the RGB compositions the white pixels correspond to cloud masked, that will be considered as NoData in the calculation of areas.

encompassing 96.29% in 1989–2005 and 99.18% of the low-risk transitions throughout the study period, indicating the stability of core forest areas despite the surrounding fragmentation dynamic.

4. Discussion

Similarly to Cho et al. (2022), who used the spectral bands of Landsat products and derived vegetation indices, obtaining 17 predictors for classification, we generated 31 datasets, considering spectral bands,

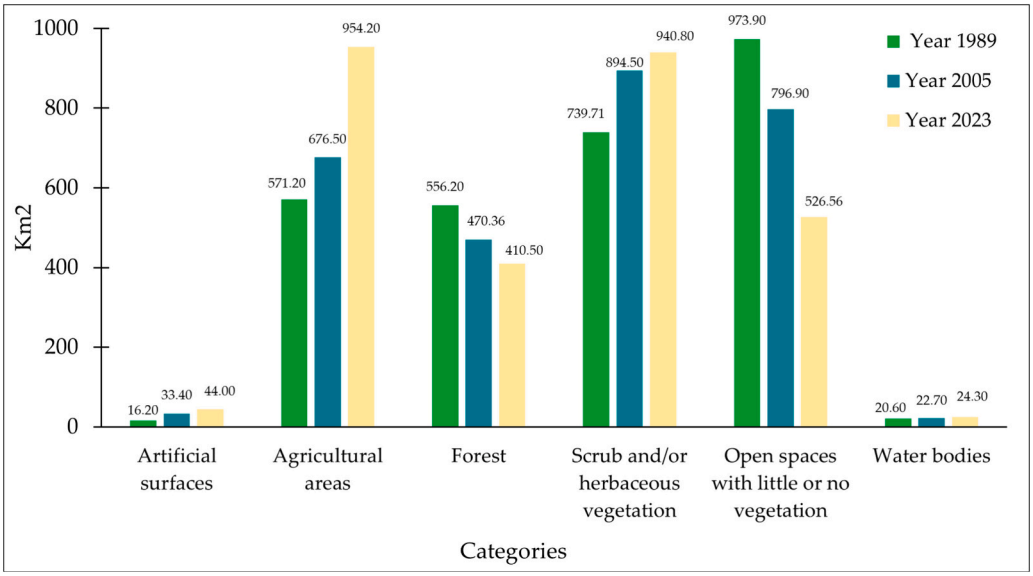

Fig. 9. Coverage in square kilometers of LULC classes for 1989, 2005 and 2023.

Table 8
LULC changes for 1989, 2005 and 2023.

	1989		2005		2023		Gains and losses (Km^2)		
	Km^2	%	Km^2	%	Km^2	%	1989 to 2005	2005 to 2023	1989 to 2023
Artificial surfaces	16.20	**0.56**	33.40	**1.15**	44.00	**1.51**	17.20	10.60	27.80
Agricultural areas	571.20	**19.66**	676.50	**23.29**	954.20	**32.85**	105.30	277.70	383.00
Forest	556.2	**19.15**	470.36	**16.19**	410.50	**14.13**	−85.84	−59.86	−145.70
Scrub and/or herbaceous vegetation	739.71	**25.46**	894.50	**30.79**	940.80	**32.39**	154.79	46.30	201.09
Open spaces with little or no vegetation	973.90	**33.53**	796.90	**27.43**	526.56	**18.13**	−177.00	−270.34	−447.34
Water bodies	20.60	**0.71**	22.70	**0.78**	24.30	**0.84**	2.10	1.60	3.70
NoData	27.15	**0.93**	10.60	**0.36**	4.60	**0.16**			
Total	2904.96	100	2904.96	100	2904.96	100			

Table 9
Rate of change for the periods 1989–2005, 2005–2023 and 1989–2023.

Categories	1989	2005	2023	Rate of Change		
	Km^2	Km^2	Km^2	1989 to 2005	2005 to 2023	1989 to 2023
Artificial surfaces	22.73	20.82	24.41	4.52%	1.53%	2.94%
Agricultural areas	682.88	720.18	857.13	1.06%	1.91%	1.51%
Forest	565.12	327.63	398.80	−1.05%	−0.76%	−0.89%
Scrub and/or herbaceous vegetation	589.13	766.17	703.09	1.19%	0.28%	0.71%
Open spaces with little or no vegetation	982.02	716.84	444.86	−1.25%	−2.30%	−1.81%
Water bodies	14.23	32.82	44.03	0.61%	0.38%	0.49%
NoData	48.84	320.50	432.64			
Total	2904.96	2904.96	2904.96			

vegetation, soil and water indices and clusters, with the objective of determining which combination yields the highest accuracies.

We run Random Forest in GEE, as it is one of the best machine learning classifiers (Gómez Fernández et al., 2022), in turn, supported by Talukdar et al. (2020), through an evaluation of six LULC classifiers determined that Random Forest is the best classifier but still needs to be tested in different morphoclimatic conditions.

The accuracies of the maps vary according to the input parameters, and various factors must be considered, in our case, on average the 31 datasets had OA between 0.33 and 0.92 and KI between 0.2 and 0.90, while Rwanga et al. (2017), who classified Landsat 8 images, considering similar LULC classes as our research, but obtained OA and KI of 0.817 and 0.722, respectively. On the other hand, Aghababaei et al. (2021) in multitemporal image classification obtained a kappa index of 0.74 and an overall accuracy of 0.81.

Nowadays, analyses of variance are very useful to identify sources of variability in the data, and to determine if these sources have a significant effect on the accuracy of the maps, for example, Lin et al. (2015), analyzed the impact of atmospheric correction and pansharpening on the accuracy of LULC classification using a two-factor factorial design and determined that atmospheric correction was statistically insignificant, while pansharpening and the interaction with atmospheric correction were statistically significant. On the other hand, Hua (2017), analyzed land cover changes and their impact on water quality, and through an ANOVA between LULC and water quality data concluded that the built-up area significantly contaminated water quality.

In this research, through an ANOVA we determined the significant differences of the 31 datasets, because the accuracies were almost high, concluding that, if there were significant differences with a confidence level of 95%, it was decided to use the inputs of the most accurate

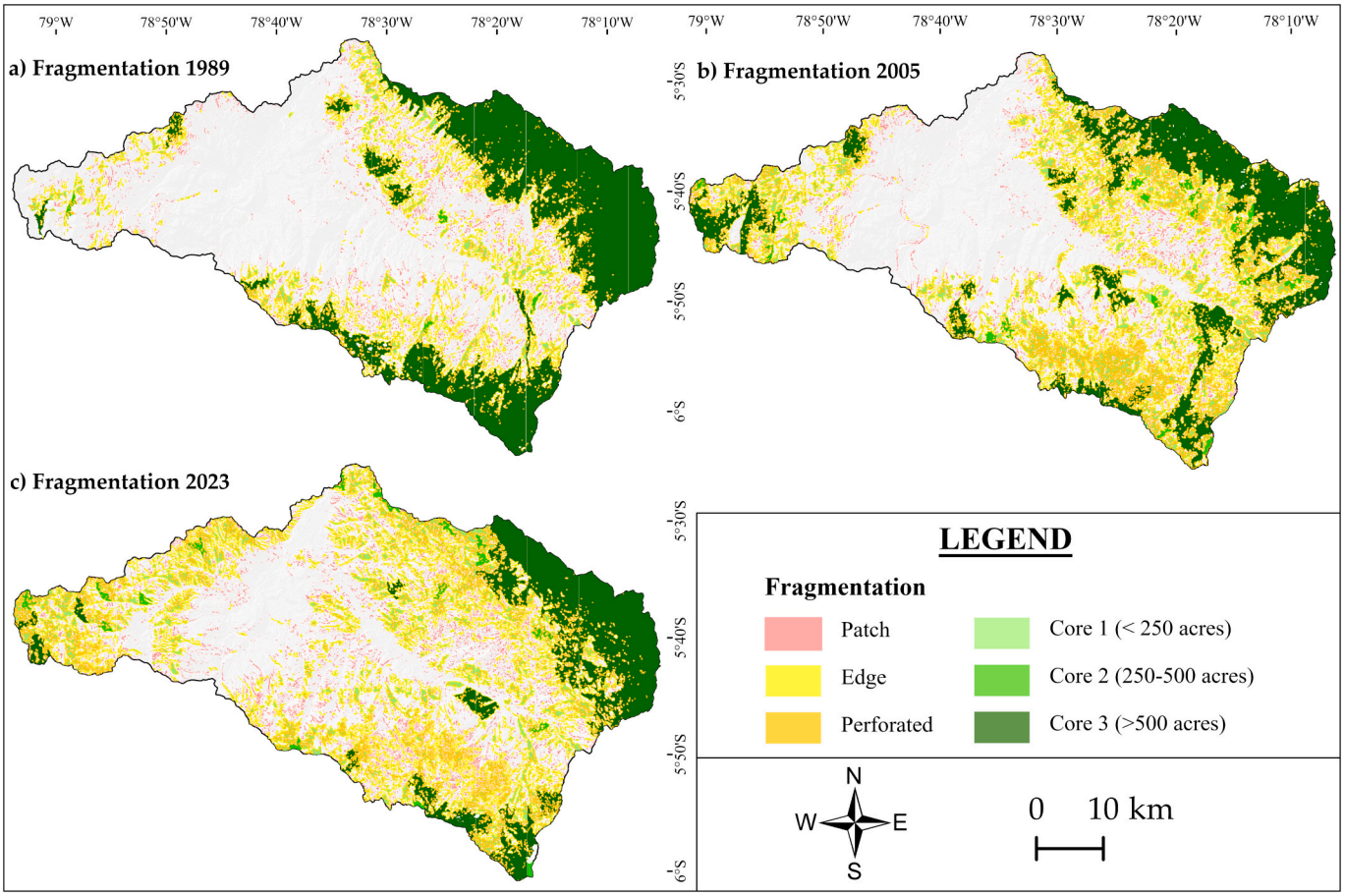

Fig. 10. Fragmentation's levels for 1989, 2005 and 2023.

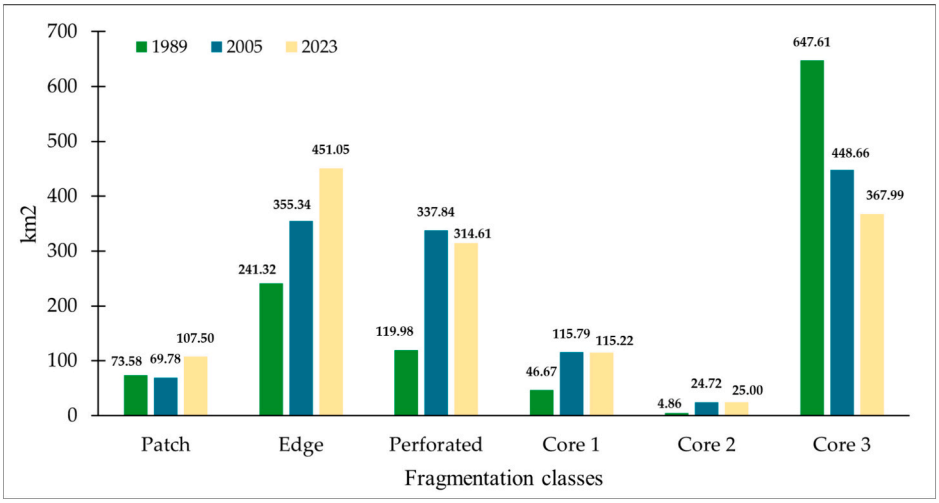

Fig. 11. Coverage of fragmentation classes for 1989, 2005 and 2023.

dataset.

The rates of changes of LULC categories vary based on the analysis period (Arunyawat and Shrestha, 2016; Talukdar et al., 2020), for example, Traore et al. (2021), determined that, the Bare Ground drastically decreased (−155.83), while, the Artificialized and Forested area increased (137.06 and 8. 44%, respectively, since 1986 to 2017), in our case, since 1989 to 2023: Open spaces with little or no vegetation decreased −1.81% per year, while Artificial surfaces increased 2.94% per year, along with Agricultural areas (1.51%). However, Forests decreased −0.89% per year, as shown in Table 9 and Fig. 9, Forest losses and Open spaces with little or no vegetation transformations are linked to the rise of Agricultural areas, and artificial surfaces.

Globally, due to fragmentation, forests have decreased in size and cover, while the total number of forest fragments has increased (Encisa-Garcia et al., 2020; Taubert et al., 2018), this phenomenon brings about changes in the composition of plant communities, with these changes

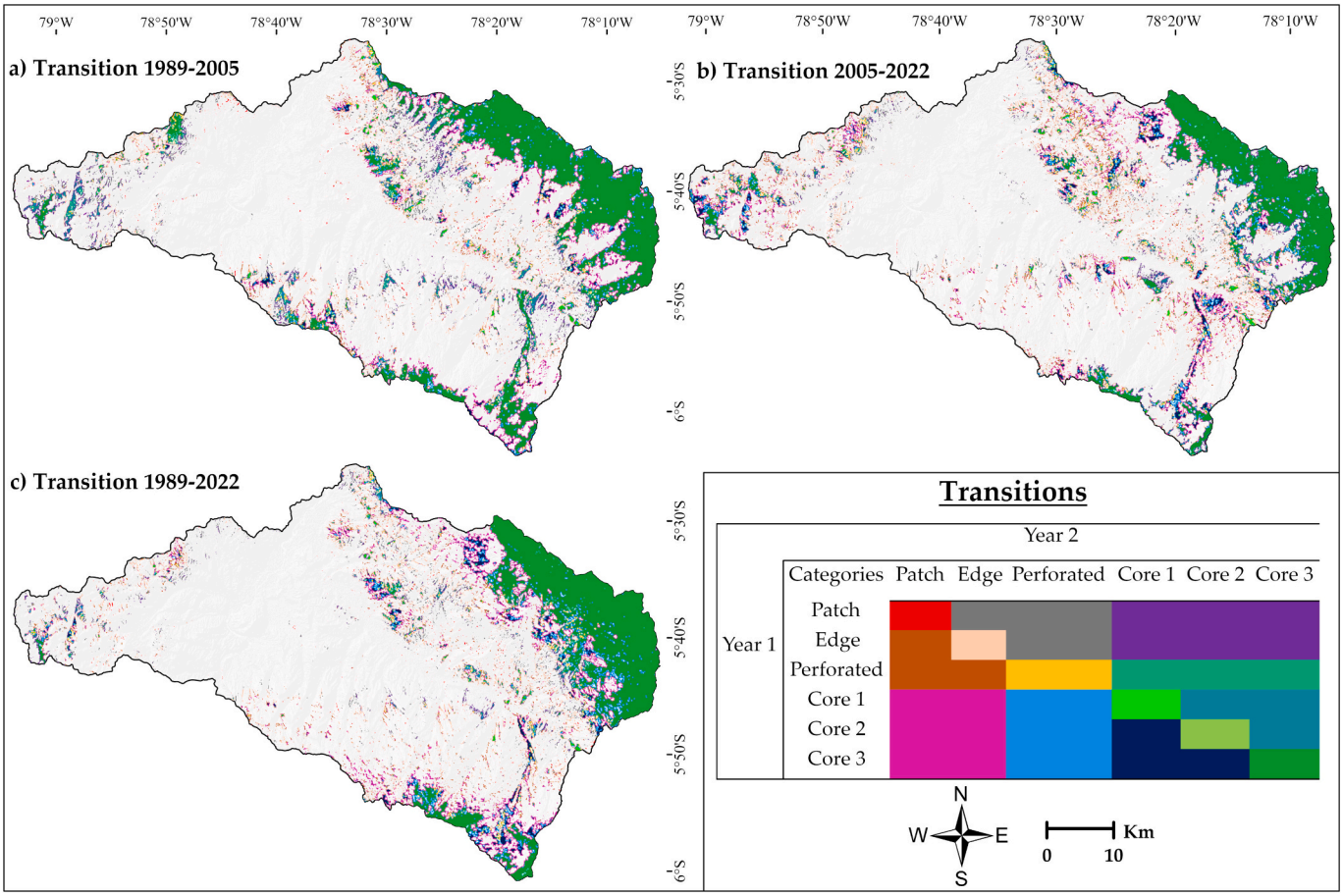

Fig. 12. Transitions of fragmentation categories for the 3 periods of analysis.

Table 10
Risk levels and covered area (km^2) for each fragmentation category transition.

Color	Description	Risk level	1989-2005		2005-2023		1989-2023	
			Area	%	Area	%	Area	%
	Patches unchanged.	****	7.08	6.57	5.28	2.90	5.66	4.21
	Core 1, 2, or 3 to Patches and Edges.	****	71.96	66.76	84.47	46.31	86.93	64.62
	Edge to Patch and Perforated to Patch and/or Edge.	****	28.75	26.67	92.65	50.79	41.92	31.17
	Total		**107.79**	100.00	**182.40**	100.00	**134.5**	100.00
	Edge unchanged.	***	63.79	21.44	88.41	27.68	66.08	24.91
	Perforated unchanged.	***	30.77	10.34	70.90	22.19	24.17	9.11
	Patch to Edge and/or Perforated and Edge to Perforated.	***	70.66	23.75	69.18	21.66	56.55	21.32
	Core 1, 2, or 3 to Perforated.	***	132.34	44.48	90.96	28.47	118.50	44.66
	Total		**297.56**	100.00	**319.45**	100.00	**265.30**	100.00
	Core 1 unchanged.	**	9.47	6.47	12.73	7.46	5.96	6.21
	Patches and edges to Core 1, 2, or 3.	**	59.26	40.48	50.86	29.78	27.65	28.84
	Perforated to Core 1, 2, or 3.	**	35.12	23.99	73.54	43.05	22.92	23.92
	Core 2 to Core 1 and Core 3 to Core 1 or 2.	**	42.53	29.06	33.68	19.72	39.32	41.02
	Total		**146.37**	100.00	**170.82**	100.00	**95.85**	100.00
	Core 2 unchanged.	*	0.00	0.00	1.12	0.44	0.17	0.05
	Core 3 unchanged.	*	317.92	96.29	234.06	92.37	321.70	99.18
	Core 1 to Core 2 and Core 1, 2 to Core 3.	*	12.26	3.71	18.23	7.19	2.48	0.76
	Total		**330.18**	100.00	**253.40**	100.00	**324.36**	100.00

are more pronounced in highly fragmented habitats compared to less fragmented ones (Collins et al., 2017), in addition, fragmentation can also affect seed dispersal (Dener et al., 2021).

Deforestation often brings with it various changes, for example variation in surface temperature, Traore et al. (2021), quantified the LULC changes and their relationship with the surface temperature changes, being the built-up areas and bare soils those areas that presented higher temperatures with respect to the vegetation and bodies of water.

Identifying the drivers of deforestation is feasible through co-occurrence and supply chain analysis, as in the case of Cho et al. (2022), who analyzed deforestation and its relationship with rubber

production, concluding that rubber production may be driving deforestation, which may have a negative impact on the environment. Similarly, future research should assess deforestation and its relationship with the advancement of the agricultural frontier in northwest Peru.

It should be noted that changes in land use aren't always negative, many times the expansion of agricultural land has a positive impact on the economy of farmers, for example, Appelt et al. (2022), through a systematic review, evaluated the socioeconomic results, the possible compensations and synergies of changes in the use of agricultural land in Southeast Asia, finding positive impacts for income and employment, negative impacts for food security, equality of gender and economic, and mixed impacts in the health sector.

As shown in Fig. 1, the study area is located in a tropical zone with altitudes between 351 and 3684 m.a.s.l, which leads to high cloud cover, but thanks to filter and masking functions in GEE it was possible to obtain mosaics with minimal cloud cover. In addition, the calculation of spectral indices and the generation of clusters was fast and flexible due to the strength of GEE, so that this research, despite the limitations, presents substantial information for the study area.

In synthesis, the present research provides substantial information for land management, reporting LULC changes, as well as landscape fragmentation levels, thus becoming a starting point for future research such as, identification of deforestation drivers, impact of deforestation on local economy, environmental quality of agricultural zone, evaluation of map accuracies using other classifiers, relationship of LULC changes and climatic anomalies etc.

5. Conclusions

We identified the optimal dataset for generating accurate LULC maps for the years 1989, 2005, and 2023, based on statistical tests applied to the results from 31 datasets and 9 types of decision trees. Our analysis determined that using between 10 and 400 decision trees in Random Forest classification doesn't significantly affect overall accuracy or the Kappa index. However, we observed a slight cumulative increase in accuracy metrics when using 100 decision trees. Therefore, we recommend using 100 decision trees for the Random Forest classifier and selecting Dataset 19 (spectral bands, soil, and water indices) as input bands for areas similar to our study area.

We show graphically and numerically the changes, fragmentation and rate of change of the LULC categories, being Artificial surfaces (2.94%) and Agricultural areas (1.51%) the ones with the highest positive rate, on the other hand, Forest (−0.89%) and Open spaces with little or no vegetation (−1.81%) present negative rates. Finally, it was determined that the coverage of level 3 forests cores decreased, and consequently, the coverage by patches and level 1 cores increased, thus showing a fragmentation of the landscape in the study area.

CRediT authorship contribution statement

Darwin Gómez-Fernández: Conceptualization, Data curation, Formal analysis, Investigation, Methodology, Software, Visualization, Writing – original draft. **Rolando Salas López:** Investigation, Project administration, Resources, Software, Supervision, Visualization. **Jhon A. Zabaleta-Santisteban:** Data curation, Formal analysis, Investigation, Software, Visualization. **Angel J. Medina-Medina:** Data curation, Formal analysis, Investigation, Software, Visualization. **Jhonsy O. Silva-López:** Investigation, Software, Validation, Writing – review & editing. **Manuel Oliva-Cruz:** Investigation, Project administration, Resources. **Nilton B. Rojas-Briceño:** Investigation, Software, Validation, Writing – review & editing.

Declaration of Generative AI and AI-assisted technologies in the writing process

During the preparation of this work the authors used Chat GPT in order to improve readability and language. After using this tool, the authors reviewed and edited the content as needed and take) full responsibility for the content of the publication.

Data availability

The code of classification, ANOVA, and the results of the Tukey's Test are available in the following web repository: https://github.com/dargofer/Fragmentation_Peru.

Acknowledgements

The authors acknowledge and thank INDES-CES of the Universidad Nacional Toribio Rodríguez de Mendoza de Amazonas (UNTRM) for its support. And the Yanayacu Experimental Center, Direction of Supervision and Monitoring in Agricultural Experimental Stations, National Institute for Agrarian Innovation (INIA).

References

Abdullah, A.Y.M., Masrur, A., Gani Adnan, M.S., Al Baky, M.A., Hassan, Q.K., Dewan, A., 2019. Spatio-temporal patterns of land use/land cover change in the heterogeneous coastal region of Bangladesh between 1990 and 2017. Remote Sens. 11 (7) https://doi.org/10.3390/rs11070790.

Aghababaei, M., Ebrahimi, A., Naghipour, A.A., Asadi, E., Verrelst, J., 2021. Vegetation types mapping using multi-temporal Landsat images in the Google earth engine platform. Remote Sens. 13 (22), 4683. https://doi.org/10.3390/RS13224683.

Appelt, J.L., Garcia Rojas, D.C., Verburg, P.H., van Vliet, J., 2022. Socioeconomic outcomes of agricultural land use change in Southeast Asia. Ambio 51 (5), 1094–1109. https://doi.org/10.1007/S13280-022-01712-4/TABLES/3.

Arunyawat, S., Shrestha, R.P., 2016. Assessing land use change and its impact on ecosystem Services in Northern Thailand. Sustainability 8 (8), 768. https://doi.org/10.3390/SU8080768.

Ban, N.C., Gurney, G.G., Marshall, N.A., Whitney, C.K., Mills, M., Gelcich, S., Bennett, N. J., Meehan, M.C., Butler, C., Ban, S., Tran, T.C., Cox, M.E., Breslow, S.J., 2019. Well-being outcomes of marine protected areas. Nat. Sustain. 2 (6), 524–532. https://doi.org/10.1038/s41893-019-0306-2.

Bao, Z., Shifaw, E., Deng, C., Sha, J., Li, X., Hanchiso, T., Yang, W., 2022. Remote sensing-based assessment of ecosystem health by optimizing vigor-organization-resilience model: A case study in Fuzhou City, China. Ecol. Inform. 72, 101889 https://doi.org/10.1016/J.ECOINF.2022.101889.

Blissag, B., Yebdri, D., Kessar, C., 2024. Spatiotemporal change analysis of LULC using remote sensing and CA-ANN approach in the Hodna basin, NE of Algeria. Phys. Chem. Earth Parts A/B/C 133, 103535. https://doi.org/10.1016/J.PCE.2023.103535.

Chamberlain, J.L., Darr, D., Meinhold, K., 2020. Rediscovering the contributions of forests and trees to transition global food systems. Forests 11 (10), 1098. https://doi.org/10.3390/F11101098.

Chazdon, R.L., Brancalion, P.H.S., Laestadius, L., Bennett-Curry, A., Buckingham, K., Kumar, C., Moll-Rocek, J., Vieira, I.C.G., Wilson, S.J., 2016. When is a forest a forest? Forest concepts and definitions in the era of forest and landscape restoration. Ambio 45 (5), 538–550. https://doi.org/10.1007/s13280-016-0772-y.

Cho, K., Goldstein, B., Gounaridis, D., Newell, J.P., 2022. Hidden risks of deforestation in global supply chains: A study of natural rubber flows from Sri Lanka to the United States. J. Clean. Prod. 349, 131275 https://doi.org/10.1016/J.JCLEPRO.2022.131275.

Chuvieco, E., 2020. Fundamentals of Satellite Remote Sensing : An Environmental Approach (Third Edit). CRC Press. https://doi.org/10.1201/9780429506482.

Cohen, J., 1960. A coefficient of agreement for nominal scales. Educ. Psychol. Meas. 20 (1), 37–46. https://doi.org/10.1177/001316446002000104.

Collins, C.D., Banks-Leite, C., Brudvig, L.A., Foster, B.L., Cook, W.M., Damschen, E.I., Andrade, A., Austin, M., Camargo, J.L., Driscoll, D.A., Holt, R.D., Laurance, W.F., Nicholls, A.O., Orrock, J.L., 2017. Fragmentation affects plant community composition over time. Ecography 40 (1), 119–130. https://doi.org/10.1111/ECOG.02607.

Congalton, R.G., 1991. A review of assessing the accuracy of classifications of remotely sensed data. Remote Sens. Environ. 54 (5), 593–600. https://doi.org/10.1016/0034-4257(91)90048-B.

Curtis, P.G., Slay, C.M., Harris, N.L., Tyukavina, A., Hansen, M.C., 2018. Classifying drivers of global forest loss. Science 361 (6407), 1108–1111. https://doi.org/10.1126/SCIENCE.AAU3445/SUPPL_FILE/AAU3445_CURTIS_SM.PDF.

Da Ponte, E., Roch, M., Leinenkugel, P., Dech, S., Kuenzer, C., 2017. Paraguay's Atlantic Forest cover loss – satellite-based change detection and fragmentation analysis between 2003 and 2013. Appl. Geogr. 79, 37–49. https://doi.org/10.1016/J.APGEOG.2016.12.005.

DeFries, R.S., Houghton, R.A., Hansen, M.C., Field, C.B., Skole, D., Townshend, J., 2002. Carbon emissions from tropical deforestation and regrowth based on satellite observations for the 1980s and 1990s. Proc. Natl. Acad. Sci. 99 (22), 14256–14261. https://doi.org/10.1073/PNAS.182560099.

Dener, E., Ovadia, O., Shemesh, H., Altman, A., Chen, S.C., Giladi, I., 2021. Direct and indirect effects of fragmentation on seed dispersal traits in a fragmented agricultural landscape. Agric. Ecosyst. Environ. 309, 107273 https://doi.org/10.1016/J.AGEE.2020.107273.

Do, A.N.T., Tran, H.D., Ashley, M., Nguyen, A.T., 2022. Monitoring landscape fragmentation and aboveground biomass estimation in can Gio mangrove biosphere reserve over the past 20 years. Eco. Inform. 70, 101743 https://doi.org/10.1016/J.ECOINF.2022.101743.

Ellis, E.C., Ramankutty, N., 2008. Putting people in the map: anthropogenic biomes of the world. Front. Ecol. Environ. 6 (8), 439–447. https://doi.org/10.1890/070062.

Encisa-Garcia, J.O., Pulhin, J.M., Cruz, R.V.O., Simondac-Peria, A.C., Ramirez, M.A.M., De Luna, C.C., 2020. Land use/land cover changes assessment and forest fragmentation analysis in the baroro river watershed, La Union, Philippines. J. Environ. Sci. Manag. SI-2, 14–27.

Fahrig, L., 2003. Effects of habitat fragmentation on biodiversity, 34, 487–515. https://doi.org/10.1146/ANNUREV.ECOLSYS.34.011802.132419.

Food and Agriculture Organization of the United Nations, 1993. Forest Resources Assessment 1990: Tropical Countries. Food and Agriculture Organization of the United Nations. https://www.fao.org/3/t0830e/T0830E00.htm.

Foody, G.M., 2020. Explaining the unsuitability of the kappa coefficient in the assessment and comparison of the accuracy of thematic maps obtained by image classification. Remote Sens. Environ. 239, 111630 https://doi.org/10.1016/J.RSE.2019.111630.

Ganivet, E., Bloomberg, M., 2019. Towards rapid assessments of tree species diversity and structure in fragmented tropical forests: a review of perspectives offered by remotely-sensed and field-based data. For. Ecol. Manag. 432 (April 2018), 40–53. https://doi.org/10.1016/j.foreco.2018.09.003.

Gao, X., Huete, A.R., Didan, K., 2003. Multisensor comparisons and validation of MODIS vegetation indices at the semiarid jornada experimental range. IEEE Trans. Geosci. Remote Sens. 41 (10 PART I), 2368–2381. https://doi.org/10.1109/TGRS.2003.813840.

Garcia, N., Alírio, J., Silva, D., Campos, J.C., Duarte, L., Arenas-Castro, S., Pôças, I., Sillero, N., Teodoro, A.C., 2023. MontObEO, Montesinho biodiversity observatory: an earth observation tool for biodiversity conservation. In: Earth Resources and Environmental Remote Sensing/GIS Applications XIV, 12734, pp. 335–345. https://doi.org/10.1117/12.2678524.

Ge, Y., Hu, S., Ren, Z., Jia, Y., Wang, J., Liu, M., Zhang, D., Zhao, W., Luo, Y., Fu, Y., Bai, H., Chen, Y., 2019. Mapping annual land use changes in China's poverty-stricken areas from 2013 to 2018. Remote Sens. Environ. 232, 111285 https://doi.org/10.1016/J.RSE.2019.111285.

Gibson, L., Lynam, A.J., Bradshaw, C.J.A., He, F., Bickford, D.P., Woodruff, D.S., Bumrungsri, S., Laurance, W.F., 2013. Near-complete extinction of native small mammal fauna 25 years after forest fragmentation. Science 341 (6153), 1508–1510. https://doi.org/10.1126/SCIENCE.1240495/SUPPL_FILE/GIBSON.SM.PDF.

Gobierno Regional de Amazonas (GOREA), Instituto de Investigaciones de la Amazonía Peruana (IIAP), 2007. Zonificación ecológica y económica del departamento de amazonas, p. 199. http://iiap.org.pe/Archivos/publicaciones/PUBL520.pdf.

Gobierno Regional de Cajamarca (GRC), 2010. Zonificacion Ecologica y Economica Como Base Para El Ordenamiento Territorial Del Departamento De Cajamarca, p. 281. https://siar.regioncajamarca.gob.pe/download/file/fid/46644.

Gómez Fernández, D., Salas López, R., Rojas Briceño, N.B., Silva López, J.O., Oliva, M., 2022. Dynamics of the Burlan and Pomacochas Lakes using SAR data in GEE, machine learning classifiers, and regression methods. ISPRS Int. J. Geo Inf. 11 (11), 534. https://doi.org/10.3390/IJGI11110534/S1.

Gong, C., Yu, S., Joesting, H., Chen, J., 2013. Determining socioeconomic drivers of urban forest fragmentation with historical remote sensing images. Landsc. Urban Plan. 117, 57–65. https://doi.org/10.1016/J.LANDURBPLAN.2013.04.009.

Gorelick, N., Hancher, M., Dixon, M., Ilyushchenko, S., Thau, D., Moore, R., 2017. Google earth engine: planetary-scale geospatial analysis for everyone. Remote Sens. Environ. 202, 18–27. https://doi.org/10.1016/j.rse.2017.06.031.

Gu, C., Zhao, P., Chen, Q., Li, S., Li, L., Liu, L., Zhang, Y., 2020. Forest cover change and the effectiveness of protected areas in the Himalaya since 1998. Sustainability 12 (15), 6123. https://doi.org/10.3390/SU12156123.

Haddad, N.M., Brudvig, L.A., Clobert, J., Davies, K.F., Gonzalez, A., Holt, R.D., Lovejoy, T.E., Sexton, J.O., Austin, M.P., Collins, C.D., Cook, W.M., Damschen, E.I., Ewers, R.M., Foster, B.L., Jenkins, C.N., King, A.J., Laurance, W.F., Levey, D.J., Margules, C.R., Townshend, J.R., 2015. Habitat fragmentation and its lasting impact on Earth's ecosystems. Sci. Adv. 1 (2) https://doi.org/10.1126/SCIADV.1500052/SUPPL_FILE/E1500052_SM.PDF.

Hansen, M.C., Potapov, P.V., Moore, R., Hancher, M., Turubanova, S.A., Tyukavina, A., Thau, D., Stehman, S.V., Goetz, S.J., Loveland, T.R., Kommareddy, A., Egorov, A., Chini, L., Justice, C.O., Townshend, J.R.G., 2013. High-resolution global maps of 21st-century forest cover change. Science (New York, N.Y.) 342 (6160), 850–853. https://doi.org/10.1126/SCIENCE.1244693.

Hassan, M.M., Duveneck, M., Southworth, J., 2023. The role of the refugee crises in driving forest cover change and fragmentation in Teknaf, Bangladesh. Ecol. Inform. 74, 101966 https://doi.org/10.1016/J.ECOINF.2022.101966.

Hay, A.M., 1979. Sampling designs to test land-use map accuracy. Photogramm. Eng. Remote. Sens. 45, 529–533. https://api.semanticscholar.org/CorpusID:131241764.

Hermosilla, T., Wulder, M.A., White, J.C., Coops, N.C., Pickell, P.D., Bolton, D.K., 2019. Impact of time on interpretations of forest fragmentation: three-decades of fragmentation dynamics over Canada. Remote Sens. Environ. 222 (September 2018), 65–77. https://doi.org/10.1016/j.rse.2018.12.027.

Hua, A.K., 2017. Land use land cover changes in detection of water quality: a study based on remote sensing and multivariate statistics. J. Environ. Public Health 2017, 12. https://doi.org/10.1155/2017/7515130.

Huang, C., Goward, S.N., Masek, J.G., Thomas, N., Zhu, Z., Vogelmann, J.E., 2010. An automated approach for reconstructing recent forest disturbance history using dense Landsat time series stacks. Remote Sens. Environ. 114 (1), 183–198. https://doi.org/10.1016/J.RSE.2009.08.017.

Huete, A.R., 1988. A soil-adjusted vegetation index (SAVI). Remote Sens. Environ. 25 (3), 295–309. https://doi.org/10.1016/0034-4257(88)90106-X.

Hysa, A., Başkaya, F.A.T., 2017. Landscape fragmentation assessment utilizing the matrix green toolbox and corine land cover data. J. Digit. Landscape Architect. 2017 (2), 54–62. https://doi.org/10.14627/537629006.

Jaramillo, J.J., Rivas, C.A., Oteros, J., Navarro-Cerrillo, R.M., 2023. Forest fragmentation and landscape connectivity changes in Ecuadorian mangroves: some hope for the future? Applied Sciences (Switzerland) 13 (8), 5001. https://doi.org/10.3390/APP13085001/S1.

Jin-Ming, Y., Li-Gang, M., Cheng-Zhi, L., Yang, L., Jian-li, D., Sheng-Tian, Y., 2019. Temporal-spatial variations and influencing factors of lakes in inland arid areas from 2000 to 2017: a case study in Xinjiang. Geomat. Nat. Haz. Risk 10 (1), 519–543. https://doi.org/10.1080/19475705.2018.1531942.

Kanade, R., John, R., 2018. Topographical influence on recent deforestation and degradation in the Sikkim Himalaya in India; implications for conservation of east Himalayan broadleaf forest. Appl. Geogr. 92, 85–93. https://doi.org/10.1016/J.APGEOG.2018.02.004.

Kennedy, R.E., Yang, Z., Gorelick, N., Braaten, J., Cavalcante, L., Cohen, W.B., Healey, S., 2018. Implementation of the LandTrendr algorithm on Google earth engine. Remote Sens. 10 (5), 1–10. https://doi.org/10.3390/rs10050691.

Landis, J.R., Koch, G.G., 1977. The measurement of observer agreement for categorical data. Biometrics 33 (1), 159. https://doi.org/10.2307/2529310.

Lin, C., Wu, C.C., Tsogt, K., Ouyang, Y.C., Chang, C.I., 2015. Effects of atmospheric correction and pansharpening on LULC classification accuracy using WorldView-2 imagery. Inform. Proc. Agriculture 2 (1), 25–36. https://doi.org/10.1016/J.INPA.2015.01.003.

Masek, J.G., Vermote, E.F., Saleous, N.E., Wolfe, R., Hall, F.G., Huemmrich, K.F., Gao, F., Kutler, J., Lim, T.K., 2006. A landsat surface reflectance dataset for North America, 1990-2000. IEEE Geosci. Remote Sens. Lett. 3 (1), 68–72. https://doi.org/10.1109/LGRS.2005.857030.

McFeeters, S.K., 2007. The use of the normalized difference water index (NDWI) in the delineation of open water features. Int. J. Remote Sens. 17 (7), 1425–1432. https://doi.org/10.1080/01431169608948714.

MIDAGRI, 2021. Atlas de la superficie agrícola del Perú. https://siea.midagri.gob.pe/portal/informativos/superficie-agricola-peruana.

Myroniuk, V., Kutia, M., Sarkissian, J., Bilous, A., Liu, S., 2020. Regional-scale Forest mapping over fragmented landscapes using global Forest products and Landsat time series classification. Remote Sens. 12 (1), 187. https://doi.org/10.3390/rs12010187.

Nagendra, H., Paul, S., Pareeth, S., Dutt, S., 2009. Landscapes of protection: forest change and fragmentation in northern West Bengal, India. Environ. Manag. 44 (5), 853–864. https://doi.org/10.1007/S00267-009-9374-9.

Negi, V.S., Pathak, R., Rawal, R.S., Bhatt, I.D., Sharma, S., 2019. Long-term ecological monitoring on forest ecosystems in Indian Himalayan region: criteria and indicator approach. Ecol. Indic. 102 (July 2018), 374–381. https://doi.org/10.1016/j.ecolind.2019.02.035.

Newman, M.E., McLaren, K.P., Wilson, B.S., 2014. Assessing deforestation and fragmentation in a tropical moist forest over 68 years; the impact of roads and legal protection in the cockpit country, Jamaica. For. Ecol. Manag. 315, 138–152. https://doi.org/10.1016/J.FORECO.2013.12.033.

Numata, I., Cochrane, M.A., Souza, C.M., Sales, M.H., 2011. Carbon emissions from deforestation and forest fragmentation in the Brazilian Amazon. Environ. Res. Lett. 6 (4) https://doi.org/10.1088/1748-9326/6/4/044003.

Ouma, Y., Nkwae, B., Moalafhi, D., Odirile, P., Parida, B., Anderson, G., Qi, J., 2022. Comparison of machine learning classifiers for multitemporal and multisensor mapping of urban LULC features. Int. Arch. Photogramm. Remote. Sens. Spat. Inf. Sci. XLIII-B3-2, 681–689. https://doi.org/10.5194/isprs-archives-XLIII-B3-2022-681-2022.

Pardini, R., de Bueno, A.A., Gardner, T.A., Prado, P.I., Metzger, J.P., 2010. Beyond the fragmentation threshold hypothesis: regime shifts in biodiversity across fragmented landscapes. PLoS One 5 (10), e13666. https://doi.org/10.1371/JOURNAL.PONE.0013666.

Parente, L., Ferreira, L., 2018. Assessing the spatial and occupation dynamics of the Brazilian pasturelands based on the automated classification of MODIS images from 2000 to 2016. Remote Sens. 10 (4) https://doi.org/10.3390/rs10040606.

Puyravaud, J.P., 2003. Standardizing the calculation of the annual rate of deforestation. For. Ecol. Manag. 177, 593–596. https://doi.org/10.1016/S0378-1127(02)00335-3.

Reddy, C.S., Sreelekshmi, S., Jha, C.S., Dadhwal, V.K., 2013. National assessment of forest fragmentation in India: landscape indices as measures of the effects of fragmentation and forest cover change. Ecol. Eng. 60, 453–464. https://doi.org/10.1016/J.ECOLENG.2013.09.064.

Rikimaru, A., Roy, P.S., Miyatake, S., 2002. Tropical forest cover density mapping. Trop. Ecol. 43 (1), 39–47.

Rocha-Santos, L., Pessoa, M.S., Cassano, C.R., Talora, D.C., Orihuela, R.L.L., Mariano-Neto, E., Morante-Filho, J.C., Faria, D., Cazetta, E., 2016. The shrinkage of a forest: landscape-scale deforestation leading to overall changes in local forest structure. Biol. Conserv. 196, 1–9. https://doi.org/10.1016/J.BIOCON.2016.01.028.

Rojas Briceño, N.B., Barboza Castillo, E., Maicelo Quintana, J.L., Oliva Cruz, S.M., Salas López, R., 2019. Deforestación en la Amazonía peruana: índices de cambios de cobertura y uso del suelo basado en SIG. Boletín de La Asociación de Geógrafos Españoles 81, 1–34. https://doi.org/10.21138/bage.2538a.

Rouse, J., Hass, R., Schell, J., Deering, D.W., 1974. Monitoring vegetation systems in the great plains with ERTS. NASA Spec. Publ. 351 (1), 309.
Rwanga, S.S., Ndambuki, J.M., Rwanga, S.S., Ndambuki, J.M., 2017. Accuracy assessment of land use/land cover classification using remote sensing and GIS. Int. J. Geosci. 8 (4), 611–622. https://doi.org/10.4236/IJG.2017.84033.
Schwartz, N.B., Budsock, A.M., Uriarte, M., 2019. Fragmentation, forest structure, and topography modulate impacts of drought in a tropical forest landscape. Ecology 100 (6). https://doi.org/10.1002/ecy.2677.
SENAMHI, 2020. Mapa climático del Perú. https://www.senamhi.gob.pe/?p=mapa-climatico-del-peru.
Shen, W., Li, M., Huang, C., Tao, X., Li, S., Wei, A., 2019. Mapping annual Forest change due to afforestation in Guangdong Province of China using active and passive remote sensing data. Remote Sens. 11 (5), 490. https://doi.org/10.3390/RS11050490.
Shetty, S., 2019. Analysis of Machine Learning Classifiers for LULC Classification on Google Earth Engine. Master's thesis. University of Twente. http://essay.utwente.nl/83543/1/shetty.pdf.
Shimizu, K., Ahmed, O.S., Ponce-Hernandez, R., Ota, T., Win, Z.C., Mizoue, N., Yoshida, S., 2017. Attribution of disturbance agents to Forest change using a Landsat time series in tropical seasonal forests in the Bago Mountains, Myanmar. Forests 8 (6), 218. https://doi.org/10.3390/f8060218.
Smith, J., Schwartz, J., 2015. Deforestation in Perú. World Wild Life. https://www.worldwildlife.org/magazine/issues/fall-2015/articles/deforestation-in-peru.
Stehman, S.V., 1997a. Estimating standard errors of accuracy assessment statistics under cluster sampling. Remote Sens. Environ. 60 (3), 258–269. https://doi.org/10.1016/S0034-4257(96)00176-9.
Stehman, S.V., 1997b. Selecting and interpreting measures of thematic classification accuracy. Remote Sens. Environ. 62 (1), 77–89. https://doi.org/10.1016/S0034-4257(97)00083-7.
Talukdar, S., Singha, P., Mahato, S., Shahfahad, Pal S., Liou, Y.A., Rahman, A., 2020. Land-use land-cover classification by machine learning classifiers for satellite observations—a review. Remote Sens. 12 (7), 1135. https://doi.org/10.3390/RS12071135.
Taubert, F., Fischer, R., Groeneveld, J., Lehmann, S., Müller, M.S., Rödig, E., Wiegand, T., Huth, A., 2018. Global patterns of tropical forest fragmentation. Nature 554 (7693), 519–522. https://doi.org/10.1038/nature25508.
Thomlinson, J.R., Bolstad, P.V., Cohen, W.B., 1999. Coordinating methodologies for scaling Landcover classifications from site-specific to global: steps toward validating global map products. Remote Sens. Environ. 70 (1), 16–28. https://doi.org/10.1016/S0034-4257(99)00055-3.
Thuiller, W., Albert, C., Araújo, M.B., Berry, P.M., Cabeza, M., Guisan, A., Hickler, T., Midgley, G.F., Paterson, J., Schurr, F.M., Sykes, M.T., Zimmermann, N.E., 2008. Predicting global change impacts on plant species' distributions: future challenges. Perspect. Plant Ecol. Evol. System. 9 (3–4), 137–152. https://doi.org/10.1016/J.PPEES.2007.09.004.
Traore, M., Lee, M.S., Rasul, A., Balew, A., 2021. Assessment of land use/land cover changes and their impacts on land surface temperature in Bangui (the capital of Central African Republic). Environ. Challeng. 4, 100114 https://doi.org/10.1016/J.ENVC.2021.100114.
Tsai, Y.H., Stow, D., An, L., Chen, H.L., Lewison, R., Shi, L., 2019. Monitoring land-cover and land-use dynamics in Fanjingshan National Nature Reserve. Appl. Geogr. 111, 102077 https://doi.org/10.1016/J.APGEOG.2019.102077.
Turner, M., 2005. Landscape ecology in North America: special feature. Ecology 86 (8), 1967–1974.
Uddin, K., Chaudhary, S., Chettri, N., Kotru, R., Murthy, M., Chaudhary, R.P., Ning, W., Shrestha, S.M., Gautam, S.K., 2015. The changing land cover and fragmenting forest on the roof of the world: a case study in Nepal's Kailash sacred landscape. Landsc. Urban Plan. 141, 1–10. https://doi.org/10.1016/J.LANDURBPLAN.2015.04.003.
Vermote, E., Justice, C., Claverie, M., Franch, B., 2016. Preliminary analysis of the performance of the Landsat 8/OLI land surface reflectance product. Remote Sens. Environ. 185, 46–56. https://doi.org/10.1016/J.RSE.2016.04.008.
Vogeler, J.C., Slesak, R.A., Fekety, P.A., Falkowski, M.J., 2020. Characterizing over four decades of forest disturbance in Minnesota, USA. Forests 11 (3), 362. https://doi.org/10.3390/F11030362.
Vogt, P., Riitters, K.H., Estreguil, C., Kozak, J., Wade, T.G., Wickham, J.D., 2006. Mapping spatial patterns with morphological image processing. Landsc. Ecol. 22 (2), 171–177. https://doi.org/10.1007/S10980-006-9013-2.
Wang, S., Azzari, G., Lobell, D.B., 2019a. Crop type mapping without field-level labels: random forest transfer and unsupervised clustering techniques. Remote Sens. Environ. 222, 303–317. https://doi.org/10.1016/J.RSE.2018.12.026.
Wang, Y., Ziv, G., Adami, M., Mitchard, E., Batterman, S.A., Buermann, W., Schwantes Marimon, B., Marimon Junior, B.H., Matias Reis, S., Rodrigues, D., Galbraith, D., 2019b. Mapping tropical disturbed forests using multi-decadal 30 m optical satellite imagery. Remote Sens. Environ. 221, 474–488. https://doi.org/10.1016/J.RSE.2018.11.028.
Wilson, E.H., Sader, S.A., 2002. Detection of forest harvest type using multiple dates of Landsat TM imagery. Remote Sens. Environ. 80 (3), 385–396. https://doi.org/10.1016/S0034-4257(01)00318-2.
Wulder, M.A., White, J.C., Andrew, M.E., Seitz, N.E., Coops, N.C., 2009. Forest fragmentation, structure, and age characteristics as a legacy of forest management. For. Ecol. Manag. 258 (9), 1938–1949. https://doi.org/10.1016/j.foreco.2009.07.041.
Wulder, M.A., Masek, J.G., Cohen, W.B., Loveland, T.R., Woodcock, C.E., 2012. Opening the archive: how free data has enabled the science and monitoring promise of Landsat. Remote Sens. Environ. 122, 2–10. https://doi.org/10.1016/j.rse.2012.01.010.
Xie, Z., Phinn, S.R., Game, E.T., Pannell, D.J., Hobbs, R.J., Briggs, P.R., McDonald-Madden, E., 2019. Using Landsat observations (1988–2017) and Google earth engine to detect vegetation cover changes in rangelands - a first step towards identifying degraded lands for conservation. Remote Sens. Environ. 232, 111317 https://doi.org/10.1016/J.RSE.2019.111317.
Xun, B., Yu, D., Liu, Y., Hao, R., Sun, Y., 2014. Quantifying isolation effect of urban growth on key ecological areas. Ecol. Eng. 69, 46–54. https://doi.org/10.1016/j.ecoleng.2014.03.041.
Zhang, Y., Liu, X., Yang, Q., Liu, Z., Li, Y., 2021. Extracting frequent sequential patterns of forest landscape dynamics in fenhe river basin, northern China, from landsat time series to evaluate landscape stability. Remote Sens. 13 (19) https://doi.org/10.3390/rs13193963.
Zhu, Z., Woodcock, C.E., 2014. Continuous change detection and classification of land cover using all available Landsat data. Remote Sens. Environ. 144, 152–171. https://doi.org/10.1016/J.RSE.2014.01.011.
Zhu, Z., Wulder, M.A., Roy, D.P., Woodcock, C.E., Hansen, M.C., Radeloff, V.C., Healey, S.P., Schaaf, C., Hostert, P., Strobl, P., Pekel, J.F., Lymburner, L., Pahlevan, N., Scambos, T.A., 2019. Benefits of the free and open Landsat data policy. Remote Sens. Environ. 224, 382–385. https://doi.org/10.1016/j.rse.2019.02.016.